ORGANOMETALLICS

Article

pubs.acs.org/Organometallics

Base-Free and Bisphosphine Ligand Dialkylmanganese(II) Complexes as Precursors for Manganese Metal Deposition

Jeffrey S. Price, Preeti Chadha, and David J. H. Emslie*

Department of Chemistry and Chemical Biology, McMaster University, Hamilton, Ontario L8S 4M1, Canada

Supporting Information

ABSTRACT: The solid-state structures and the physical, solution magnetic, solid-state magnetic, and spectroscopic (NMR and UV/vis) properties of a range of oxygen- and nitrogen-free dialkylmanganese(II) complexes are reported, and the solution reactivity of these complexes toward H_2 and $ZnEt_2$ is described. The compounds investigated are $[\{Mn(\mu\text{-}CH_2SiMe_3)_2\}_\infty]$ (**1**), $[\{Mn(CH_2CMe_3)(\mu\text{-}CH_2CMe_3)_2\}_2\{Mn(\mu\text{-}CH_2CMe_3)_2Mn\}]$ (**2**), $[Mn(CH_2SiMe_3)_2(dmpe)]$ (**3**; dmpe = 1,2-bis(dimethylphosphino)ethane), $[\{Mn(CH_2CMe_3)_2(\mu\text{-}dmpe)\}_2]$ (**4**), $[\{Mn(CH_2SiMe_3)(\mu\text{-}CH_2SiMe_3)\}_2(\mu\text{-}dmpe)]$ (**5**), $[\{Mn(CH_2CMe_3)(\mu\text{-}CH_2CMe_3)\}_2(\mu\text{-}dmpe)]$ (**6**), $[\{Mn(CH_2SiMe_3)(\mu\text{-}CH_2SiMe_3)\}_2(\mu\text{-}dmpm)]$ (**7**; dmpm = bis(dimethylphosphino)methane), and $[\{Mn(CH_2CMe_3)(\mu\text{-}CH_2CMe_3)\}_2(\mu\text{-}dmpm)]$ (**8**). Syntheses for **1**−**4** have previously been reported, but the solid-state structures and most properties of **2**−**4** had not been described. Compounds **5** and **6**, with a 1:2 dmpe/Mn ratio, were prepared by reaction of **3** and **4** with base-free **1** and **2**, respectively. Compounds **7** and **8** were accessed by reaction of **1** and **2** with 0.5 equiv or more of dmpm per manganese atom. An X-ray structure of **2** revealed a tetrametallic structure with two terminal and six bridging alkyl groups. In the solid state, bisphosphine-coordinated **3**−**8** adopted three distinct structural types: (a) monometallic $[LMnR_2]$, (b) dimetallic $[R_2Mn(\mu\text{-}L)_2MnR_2]$, and (c) dimetallic $[\{RMn(\mu\text{-}R)\}_2(\mu\text{-}L)]$ (L = dmpe, dmpm). Compound **3** exhibited particularly desirable properties for an ALD or CVD precursor, melting at 62−63 °C, subliming at 60 °C (5 mTorr), and showing negligible decomposition after 24 h at 120 °C. Comparison of variable-temperature solution and solid-state magnetic data provided insight into the solution structures of **2**−**8**. Solution reactions of **1**-**8** with H_2 yielded manganese metal, demonstrating the thermodynamic feasibility of the key reaction steps required for manganese(II) dialkyl complexes to serve, in combination with H_2, as precursors for metal ALD or pulsed CVD. In contrast, the solution reactions of **1**−**8** with $ZnEt_2$ yielded a zinc−manganese alloy with an approximate 1:1 Zn/Mn ratio.

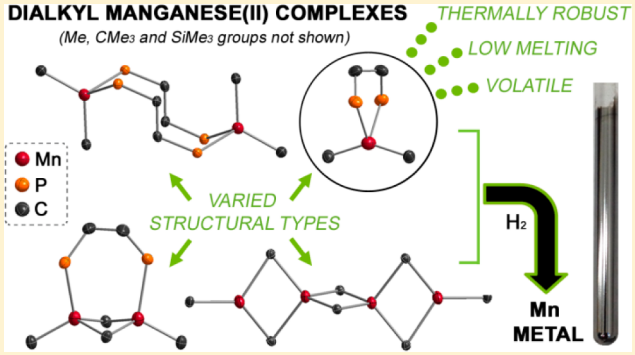

INTRODUCTION

Prominent methods for thin film deposition include electroplating, electroless deposition, physical vapor deposition (PVD), chemical vapor deposition (CVD), and atomic layer deposition (ALD).[1] Electroplating and electroless deposition are conducted in solution or a melt, whereas PVD relies upon evaporation or sputtering of the target material under vacuum, often using resistive or electron beam heating or bombardment by high-energy particles, respectively. In contrast, CVD and ALD are vapor-phase deposition techniques requiring at least one volatile molecular precursor as a source of elements in the target thin film. In CVD, the target material is formed by thermal decomposition of the volatile molecular precursor upon contact with a heated substrate. In contrast, in ALD, a volatile molecular precursor is adsorbed on the surface of a heated substrate and the resulting monolayer is reacted with a volatile coreactant (a molecular coreactant in the case of thermal ALD or plasma-generated atoms in the case of plasma-enhanced ALD) to produce a submonolayer of the target material. Precursor and coreactant pulses are separated by inert gas or vacuum purge steps, and the precursor pulse/purge/coreactant pulse/purge sequence is repeated until a film of the desired thickness is obtained.[2]

Of the thin film deposition methods described above, thermal ALD is uniquely well suited to deposit the highly uniform and conformal ultrathin films required in future microelectronic devices. For this reason, ALD is currently used to deposit HfO_2 in microprocessors, Al_2O_3 in dynamic random access memory, and ZnS in electroluminescent displays.[3] Thermal metal ALD has been reported for the following late transition metals: Cu, Ni, Pd, Pt, Co, Rh, Ir, Fe, Ru, and Os.[4] However, reports of more electropositive early- or mid-transition-metal ALD are scarce (vide infra), given that most ALD precursors contain a metal in a positive oxidation state, which must be reduced to the 0 oxidation state for metal film deposition. ALD of moderately electropositive tungsten has been achieved using WF_6 in combination with Si_2H_6,[5] SiH_4,[6] or

Received: October 29, 2015
Published: December 30, 2015

DOI: 10.1021/acs.organomet.5b00907
Organometallics 2016, 35, 168−180

B_2H_6.[6b,7] Furthermore, ALD of elemental chromium, which is significantly more electropositive ($\chi_{Pauling}$ = 1.66)[8] than tungsten, was recently reported by Winter using [Cr(OCMe^{t}BuCH=N^{t}Bu)$_2$] and $BH_3(NHMe_2)$. However, film growth was only observed on Ru/SiO_2/Si substrates, a lengthy nucleation process was required, and the film thickness plateaued at approximately 10 nm. Manganese ALD[9] was also likely achieved using [Mn_2(OCMe^{t}BuCH=N^{t}Bu)$_4$] and $BH_3(NHMe_2)$, although only MnO_x was observed after air exposure, and the same substrate, nucleation, and film growth restrictions that applied to Cr also applied to Mn.[10] Cu–Mn alloy ALD has recently been reported using a combination of [Mn_2(OCMe^{t}BuCH=N^{t}Bu)$_4$]/$BH_3(NHMe_2)$ and [Cu(dmap)$_2$]/$BH_3(NHMe_2)$ cycles (dmap = 1-dimethylamino-2-propoxide).[11] Additionally, titanium ALD was recently accomplished using $TiCl_4$ in combination with 2-methyl-1,4-bis(trimethylsilyl)-2,5-cyclohexadiene or 1,4-bis(trimethylsilyl)-1,4-dihydropyrazine.[12]

We have previously investigated the use of metal alkyl complexes (e.g., $ZnEt_2$) as coreactants for copper metal ALD,[13] and in this work we set out to determine whether highly reactive electropositive transition-metal alkyl complexes could exhibit the reactivity, volatility, and thermal stability suitable to effect electropositive metal deposition in combination with reagents such as H_2 and $ZnEt_2$ (hydrogen gas has previously been used as a coreactant for ALD of Fe,[14] Ru,[15] Co,[14] Ir,[16] Ni,[14,17] Pd,[18] and Cu;[14,19] $ZnEt_2$ has been used as a coreactant for the ALD of Cu[20]).

As ALD precursors, electropositive metal alkyl complexes offer several potential advantages relative to coordination or cyclopentadienyl complexes: (a) the high reactivity of polar metal–alkyl bonds may provide access to low-temperature reaction pathways for elemental metal deposition,[23] (b) the metal–nitrogen and metal–oxygen bonds typically encountered in coordination complexes can be avoided, precluding metal oxide or nitride formation, and (c) in reactions with H_2, the byproducts are highly unreactive and volatile alkanes which should be readily eliminated from the growing film. Transition-metal alkyl complexes have rarely been used as precursors for pulsed CVD or ALD, although notable exceptions are [$PtMe_2$(COD)][21] and [Cp′$PtMe_3$][22] (COD = 1,5-cyclooctadiene, Cp′ = methylcylcopentadienyl).

Manganese was selected as the metal of choice in the current work due to a Pauling electronegativity ($\chi_{Pauling}$ = 1.55) lower than that of all transition metals in groups 5–12, with the exception of tantalum ($\chi_{Pauling}$ = 1.5).[9] Furthermore, manganese ALD is of interest since copper–manganese alloys can be used for self-formation of a $MnSi_xO_y$ diffusion barrier at the interface between copper interconnect wiring and dielectric materials rich in silicon and oxygen.[24]

The reactivity envisaged between a dialkylmanganese precursor and H_2 or $ZnEt_2$ is shown in Scheme 1. With H_2, a mixed alkyl hydride complex (MnHR) should be accessible by σ-bond metathesis or oxidative addition of H_2 followed by reductive elimination of HR. This mixed alkyl hydride complex can be expected to be particularly susceptible to HR reductive elimination for both thermodynamic and kinetic reasons,[25] leading to manganese metal deposition. With $ZnEt_2$, stepwise alkyl exchange with MnR_2 would provide Mn(Et)R and then $MnEt_2$, which can be expected to undergo rapid β-hydride elimination to form either MnHR or MnHEt, respectively. MnHR is the same intermediate targeted in reactions with H_2, and MnHEt will decompose via either HEt reductive elimination to form manganese metal, or β-hydride elimination to form MnH_2; an unstable species observed only in low-temperature matrices.[26] While HR (R = CH_2EMe_3) is the only byproduct expected in reactions with H_2, byproducts in the reactions with $ZnEt_2$ can include ZnEtR (or ZnR_2; not shown in Scheme 1), ethylene, HR, HEt, and H_2.

Scheme 1. Possible Pathways for Mn(s) Deposition Using Dialkylmanganese(II) Complexes in Combination with H_2 or $ZnEt_2$ Coreactants

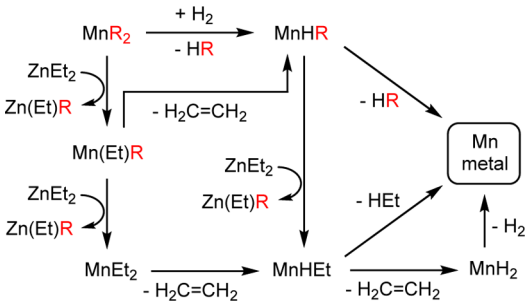

The aforementioned reactivity can only be utilized for manganese ALD or pulsed CVD if a dialkylmanganese(II) precursor with an appropriate balance of thermal stability, volatility, and reactivity can be identified. The first neutral dialkylmanganese(II) complex, $MnMe_2$, was reported by Beermann and Clauss over a half century ago, although the structure this compound, which explodes under the influence of shock or friction, remains unknown.[27] In contrast, Wilkinson et al. prepared homoleptic trimethylsilylmethyl, neopentyl, neophyl (CH_2CMe_2Ph),[28] and 1-adamantylmethyl[29] manganese(II) complexes with much greater stability due to increased steric bulk. X-ray crystal structures were reported for the trimethylsilylmethyl and neophyl complexes, which are polymeric and dimeric, respectively.[28b,30] More recently, homoleptic benzyl,[31] *o*-$CH_2C_6H_4NMe_2$,[32] bis(trimethylsilyl)methyl,[33] tris(trimethylsilyl)methyl,[34] and C(SiMe$_3$)$_2$(SiMe$_2$NMe$_2$)[35] manganese(II) complexes have also been crystallographically characterized.

Dialkylmanganese(II) complexes have been coordinated to a wide variety of Lewis bases, including PMe_3,[36] PEt_3, PMe_2Ph, $PMePh_2$, PCy_3,[37] dmpe (1,2-bis(dimethylphosphino)ethane),[36b,38] pyridine,[31,39] 2,2′-bipyridine (bipy),[31] TMEDA (*N*,*N*,*N*′,*N*′-tetramethylethylenediamine),[28] a bidentate diimine ligand (*N*,*N*′-bis(mesitylmethylene)-1,2-cyclohexanediamine),[40] sparteine,[41] THF,[31,38b,42] ^{i}Pr$_2$NC(O)CH_2Ph,[43] 1,4-dioxane,[39] and a carbene (1,3-bis(2,6-diisopropylphenyl)imidazole-2-ylidene),[44] although many of these complexes have not been structurally characterized. Dialkylmanganese(II) complexes with *o*-phenylenedimethylene (*o*-$C_6H_4(CH_2)_2^{2-}$),[36b] cyclohexyl, and *tert*-butyl[45] alkyl groups have also been isolated in combination with supporting dmpe ligands.

Herein we describe the synthesis of both new and previously reported dialkylmanganese(II) complexes (eight in total), detailed solution and solid-state characterization, including single-crystal X-ray diffraction, PXRD, NMR and UV–visible spectroscopy, and variable-temperature solution state (Evans) and solid-state (SQUID) magnetic measurements, evaluation of thermal stability and volatility, and solution reactivity studies with H_2 and $ZnEt_2$ leading to manganese metal and manganese–zinc alloy electroless deposition. This work targets base-free as well as dmpe and dmpm (bis(dimethylphosphino)methane) coordinated bis(trimethylsilylmethyl) and dineopen-

DOI: 10.1021/acs.organomet.5b00907
Organometallics 2016, 35, 168–180

tyl manganese(II) complexes, since (a) they have fairly low molecular weights and do not contain aromatic groups, maximizing the potential for appreciable volatility, (b) they do not contain β-hydrogen atoms, imparting thermal stability, (c) they are free from oxygen or nitrogen donors, precluding manganese oxide or nitride deposition, and (d) the chelate effect will help to prevent phosphine ligand dissociation during sublimation. The base-free compounds[28] and the 1:1 MnR_2/dmpe adducts[36b] have previously been reported, but an X-ray crystal structure has only been reported for $[\{Mn(\mu\text{-}CH_2SiMe_3)_2\}_\infty]$.

RESULTS AND DISCUSSION

Synthesis and X-ray Crystal Structures. Base-free bis(trimethylsilylmethyl)manganese(II) (**1**) and dineopentylmanganese(II) (**2**) were prepared via the reactions of $MnCl_2$ with $MgR_2(dioxane)_x$ (R = CH_2SiMe_3, CH_2CMe_3; x = 0.25−0.8), following modifications of the literature procedures (Scheme 2).[28b] The 1:1 Mn/dmpe (dmpe = 1,2-bis(dimethylphosphino)ethane) complexes $[Mn(CH_2SiMe_3)_2(dmpe)]$ (**3**) and $[\{Mn(CH_2CMe_3)_2(\mu\text{-}dmpe)\}_2]$ (**4**) were also prepared as previously reported (Scheme 2),[36b] while the 2:1 Mn/dmpe complexes $[\{Mn(CH_2SiMe_3)(\mu\text{-}CH_2SiMe_3)\}_2(\mu\text{-}dmpe)]$ (**5**) and $[\{Mn(CH_2CMe_3)(\mu\text{-}CH_2CMe_3)\}_2(\mu\text{-}dmpe)]$ (**6**) were synthesized by addition of 1 equiv of the corresponding base-free dialkylmanganese(II) precursor to **3** and **4**, respectively (Scheme 2). Compounds **1** and **2** reacted with bis(dimethylphosphino)methane (dmpm) to form exclusively $[\{Mn(CH_2SiMe_3)(\mu\text{-}CH_2SiMe_3)\}_2(\mu\text{-}dmpm)]$ (**7**) and $[\{Mn(CH_2CMe_3)(\mu\text{-}CH_2CMe_3)\}_2(\mu\text{-}dmpm)]$ (**8**), even when an excess of dmpm was added (Scheme 2).

Compound **4** is colorless, **3** is yellow, and **2** is dark brown, whereas **1** and **5**−**8** are red or black when crystalline and pale pink when powdered. All eight compounds display high oxygen sensitivity and were characterized by combustion elemental analysis, single-crystal X-ray diffraction (except **1**),[46] PXRD on the bulk sample, ^{1}H NMR spectroscopy (except nearly insoluble **1**), UV/vis spectroscopy (except nearly insoluble **1** and colorless **4**), and both SQUID and Evans solution magnetic measurements (except **1**) (vide infra). Additionally, melting points and sublimation temperatures were determined, and the thermal stability was assessed.

An X-ray structure has not previously been reported for base-free dineopentylmanganese(II) (**2**). However, Wilkinson et al. noted in 1976 that **2** is a tetramer in the solid state,[28b] citing a personal communication from M. B. Hursthouse and P. Raithby.[30] Additionally, an electron diffraction study was reported for **2**, revealing a monometallic structure in the vapor phase.[47] In this work, dark brown X-ray-quality crystals of **2** were obtained from hexanes at −30 °C, confirming a tetrametallic structure (Figure 1), with the two outer manganese atoms in a distorted-trigonal-planar geometry ($\sum$(C−Mn(1)−C) = 359.82(6)°; C−Mn(1)−C = 105.16(3), 122.62(3), and 132.04(4)°) and the inner manganese atoms in a distorted-tetrahedral geometry (C−Mn(2)−C = 100.06(3)−122.50(3)°). The only other neutral and homoleptic dialkylmanganese(II) complex known to contain a trigonal-planar manganese center is $[\{Mn(CH_2CMe_2Ph)(\mu\text{-}CH_2CMe_2Ph)\}_2]$,[28b,30,31] though it deviates more from planarity ($\sum$(C−Mn−C) = 354.7(1)°) than complex **2**, likely due to an η^2 interaction between each manganese atom and the phenyl ring of a bridging CH_2CMe_2Ph group. The tetrametallic structure of **2** presumably differs from the polymeric structure of **1**[28b] due to the increased steric demands of neopentyl versus trimethylsilylmethyl ligands.

Compound **2** has an inversion center between the central manganese atoms, and the terminal Mn(1)−C(1) bond distance of 2.1211(9) Å is significantly shorter than the Mn−C bonds to the bridging neopentyl ligands. For each bridging neopentyl group, one Mn−C bond is approximately 0.1−0.2 Å shorter than the other, with the short Mn−C distances ranging from 2.213(1) to 2.232(1) Å and long Mn−C distances of 2.3265(7) Å to three-coordinate Mn(1) and 2.3939(7) and 2.4092(9) Å to four-coordinate Mn(2). Bridging alkyl groups in multimetallic manganese alkyl complexes in the literature also

Scheme 2. Synthesis of Compounds 1−8

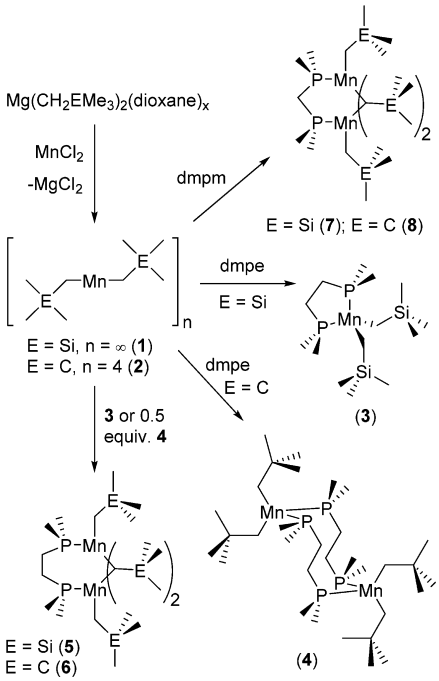

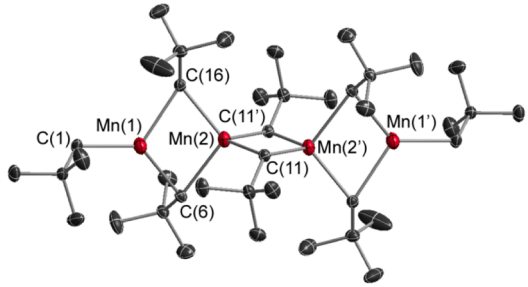

Figure 1. X-ray crystal structure for $[\{Mn(CH_2CMe_3)(\mu\text{-}CH_2CMe_3)_2\}\{Mn(\mu\text{-}CH_2CMe_3)_2Mn\}]$ (**2**). Hydrogen atoms are omitted for clarity, and ellipsoids are set to 60% (C) and 80% probability (Mn). Bond distances (Å) and angles (deg): Mn(1)···Mn(2) 2.7022(4), Mn(2)···Mn(2′) 2.7165(4), Mn(1)−C(1) 2.1211(9), Mn(1)−C(6) 2.2322(9), Mn(2)−C(16) 2.232(1), Mn(2)−C(11) 2.213(1), Mn(1)−C(16) 2.3265(7), Mn(2)−C(6) 2.3939(7), Mn(2)−C(11′) 2.4092(9); Mn(1)−C(6)−Mn(2) 71.38(3), Mn(1)−C(16)−Mn(2) 72.67(3), Mn(2)−C(11)−Mn(2′) 71.85(3), C(1)−Mn(1)−C(6) 132.04(4), C(1)−Mn(1)−C(16) 122.62(3), C(6)−Mn(1)−C(16) 105.16(3).

DOI: 10.1021/acs.organomet.5b00907
Organometallics 2016, 35, 168−180

exhibit one short and one long Mn−C bond,[48] as do all μ-alkyl manganese complexes in this work (vide infra). The Mn(1)−Mn(2) and Mn(2)−Mn(2′) distances in **2** are 2.7022(4) and 2.7165(4) Å, which are almost 0.2 Å shorter than the Mn−Mn distances previously reported for $[\{Mn(CH_2SiMe_3)_2\}_\infty]$ (**1**). Furthermore, the Mn−C−Mn angles in **2** (71.38(3)−72.67(3)°) are approximately 5° more acute than those in **1**, while the Mn−C distances are comparable.[31] The Mn−Mn distances in **2** lie between the sum of ionic (2.58 Å) and van der Waals radii (4.10 Å)[49] and are within the range previously reported (2.5−3.2 Å) for single Mn−Mn bonds in the vast majority of coordination and organometallic complexes.[48] However, they are longer than the shortest Mn−Mn distances in elemental manganese (2.26, 2.37, and 2.47 Å for α-, β-, and γ-Mn, respectively).[50]

X-ray-quality crystals of the 1:1 Mn/dmpe complexes $[Mn(CH_2SiMe_3)_2(dmpe)]$ (**3**) and $[\{Mn(CH_2CMe_3)_2(\mu\text{-dmpe})\}_2]$ (**4**) were obtained from hexanes at −30 °C. Compound **3** (Figure 2) is monometallic with a tetrahedral geometry that is distorted due to the small bite angle of dmpe (78.76(2)° in **3**). In contrast, **4** (Figure 3) is dimetallic with bridging dmpe ligands and a Mn−Mn distance of 6.756(2) Å, which is far greater than the sum of the van der Waals radii. Compound **4** features tetrahedral manganese centers (X−Mn−X = 94.79(2)−122.20(9)°; X = C, P) and a central 10-membered ring with a boat−chair−boat conformation, which is the dominant conformation of cyclodecane.[51,52] An organometallic complex featuring a similar $M_2(\mu\text{-dppe})_2$ core (dppe = bis(diphenylphosphino)ethane) has been structurally characterized for Mo.[53] The Mn−P and Mn−C distances in **3** and **4** are unremarkable, ranging from 2.6241(9) to 2.6541(5) Å (Mn−P) and from 2.1320(14) to 2.160(2) Å (Mn−C), similar to the Mn−P and $Mn-C_{terminal}$ bond lengths in **1**, **2**, $[Mn(CH_2Ph)_2(PMe_3)_2]$,[36b] and $[Mn(CH_2SiMe_3)_2(tmeda)]$ (tmeda = *N*,*N*,*N*′,*N*′-tetramethylethylenediamine).[39] In contrast, significantly longer Mn−P and Mn−C distances were reported for $[Mn\{CH(SiMe_3)_2\}_2(dmpe)]$,[38b] presumably due to greatly increased steric hindrance at the metal center.

Bright red X-ray-quality crystals of $[\{Mn(CH_2SiMe_3)(\mu\text{-}CH_2SiMe_3)\}_2(\mu\text{-dmpe})]$ (**5**) were obtained at −30 °C from both toluene and hexanes. The unit cell for the structure obtained from toluene (Figure 4) contains three independent molecules, while the structure obtained from hexanes (Figure S36 in the Supporting Information) has only one independent molecule in the unit cell. Black X-ray-quality crystals of the neopentyl analogue $[\{Mn(CH_2CMe_3)(\mu\text{-}CH_2CMe_3)\}_2(\mu\text{-dmpe})]$ (**6**) (Figure 5) were obtained from toluene at −30 °C. Both **5** and **6** are dimetallic with tetrahedral manganese centers (C−Mn−X = 94.4(1)−131.4(4)°; X = C, P) coordinated to one terminal alkyl group, two bridging alkyl groups, and one phosphorus atom of a bridging dmpe ligand. The terminal Mn−C distances in **5** and **6** (2.123(2)−2.141(5) Å in **5**; 2.160(6) and 2.18(1) Å in **6**) are shorter than the bridging Mn−C distances, and as in base-free **1** and **2**, each of the bridging alkyl groups is closer to one manganese atom than the other; the short $Mn-C_{bridging}$ distances range from 2.183(2) to 2.211(4) Å in **5** and from 2.252(5) to 2.27(1) Å in **6**, whereas the long $Mn-C_{bridging}$ distances range from 2.362(2) to 2.379(4) Å in **5** and from 2.300(9) to 2.342(6) Å in **6**.

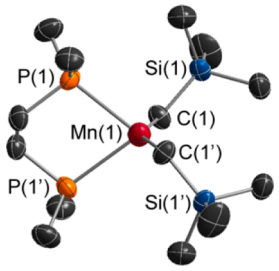

Figure 2. X-ray crystal structure for $[Mn(CH_2SiMe_3)_2(dmpe)]$ (**3**). Hydrogen atoms are omitted for clarity, and ellipsoids are set to 50% (C, P, Si) and 70% probability (Mn). All carbon atoms in the dmpe ligand are disordered over two positions, and only the dominant conformation (69%) is shown above. Bond distances (Å) and angles (deg): Mn−C 2.1320(14), Mn−P 2.6541(5); P−Mn−P 78.76(2), C−Mn−C 144.34(9), P(1)−Mn−C(1) 108.59(5), P(1)−Mn−C(1′) 98.89(4).

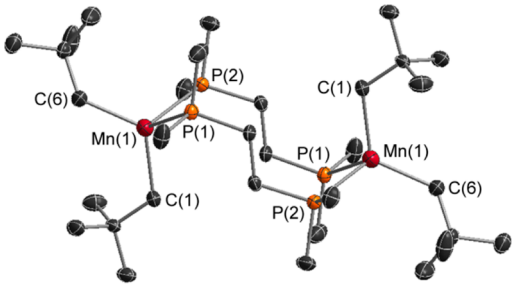

Figure 3. X-ray crystal structure for $[\{Mn(CH_2CMe_3)_2(\mu\text{-dmpe})\}_2]$ (**4**). Hydrogen atoms are omitted for clarity, and ellipsoids are set to 60% (C, P) and 80% probability (Mn). Bond distances (Å) and angles (deg): Mn···Mn 6.756(2), Mn(1)−P(1) 2.6241(9), Mn(1)−P(2′) 2.643(1), Mn(1)−C(1) 2.160(2), Mn(1)−C(6) 2.160(2); P(1)−Mn(1)−P(2) 94.79(2), C(1)−Mn(1)−C(6) 122.20(9), C(1)−Mn(1)−P(1) 104.25(7), C(6)−Mn(1)−P(1) 106.94(7), C(1)−Mn(1)−P(2) 119.20(7), C(6)−Mn−P(2) 105.25(7).

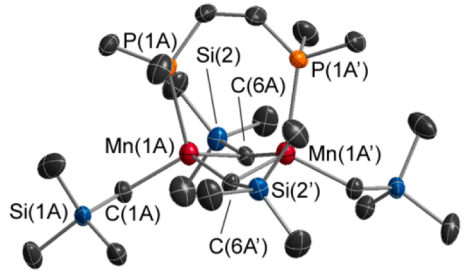

Figure 4. X-ray crystal structure for $[\{Mn(CH_2SiMe_3)(\mu\text{-}CH_2SiMe_3)\}_2(\mu\text{-dmpe})]$ (**5**) obtained by crystallization from toluene. Hydrogen atoms are omitted for clarity, and ellipsoids are set to 50% (C, P, Si) and 70% probability (Mn). The unit cell contains three independent and essentially isostructural molecules (A−C), and only molecule A is shown. Bond distances (Å) and angles (deg): Mn(1A)···Mn(1A′) 2.7202(6), Mn(1B)···Mn(1B′) 2.7177(6), Mn(1C)···Mn(1C′) 2.7322(6), Mn(1A)−P(1A) 2.6007(9), Mn(1B)−P(1B) 2.5909(9), Mn(1C)−P(1C) 2.6020(9), Mn(1A)−C(1A) 2.123(2), Mn(1B)−C(1B) 2.137(2), Mn(1C)−C(1C) 2.136(2), Mn(1A)−C(6A) 2.183(2), Mn(1B)−C(6B) 2.200(2), Mn(1C)−C(6C) 2.208(2), Mn(1A)−C(6A′) 2.366(2), Mn(1B)−C(6B′) 2.370(2), Mn(1C)−C(6C′) 2.362(2); Mn(1A)−C(6A)−Mn(1A′) 73.34(7), Mn(1B)−C(6B)−Mn(1B′) 72.88(7), Mn(1C)−C(6C)−Mn(1C′) 73.35(8). See the Supporting Information for bond distances and angles in the structure of **5** obtained from hexanes.

DOI: 10.1021/acs.organomet.5b00907
Organometallics 2016, 35, 168−180

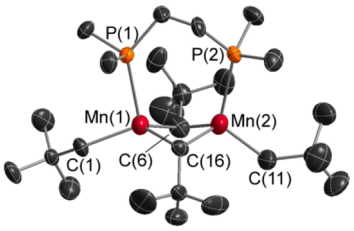

Figure 5. X-ray crystal structure for [{Mn(CH_2CMe_3)(μ-CH_2CMe_3)}$_2$(μ-dmpe)] (**6**). Hydrogen atoms are omitted for clarity, and ellipsoids are set to 50% (C, P) and 70% probability (Mn). Positions of all carbon atoms in three of the four neopentyl groups (C(1)–C(15)) are disordered over two positions. The figure shows only one position for each of the disordered groups (occupancy: 50% for C1–C5, 82% for C6–C10, and 87% for C11–C15). Bond distances (Å) and angles (deg): Mn(1)···Mn(2) 2.685(1), Mn(1)–P(1) 2.605(1), Mn(2)–P(2) 2.641(1), Mn(1)–C(1) 2.160(6), Mn(2)–C(11) 2.18(1), Mn(1)–C(16) 2.252(5), Mn(2)–C(6) 2.27(1), Mn(1)–C(6) 2.300(9), Mn(2)–C(16) 2.342(6); Mn(1)–C(6)–Mn(2) 72.0(3), Mn(1)–C(16)–Mn(2) 71.5(2).

The Mn–P distances in **5** and **6** are similar and unexceptional. However, the Mn–Mn distances of 2.7177(6)–2.7322(6) Å in **5** are shorter than those in base-free **1** by over 0.15 Å, likely due to the tethering influence of the bridging bisphosphine ligand. The Mn–C–Mn angles in **5** (72.88(7)–73.35(8)°) are also more acute than those in base-free **1** (76.82(4) and 77.19(5)°), consistent with the shorter Mn–Mn distance in the former compound. The Mn–Mn distance of 2.685(1) Å in **6** is less than 0.05 Å shorter than the corresponding distance in base-free **2**, but it is significantly shorter than the Mn–Mn distance in **5**. The Mn–$C_{terminal}$ and average Mn–$C_{bridging}$ distances (vide supra) are slightly longer in **6** than in **5**, and the Mn–C–Mn angles in **6** (71.5(2)–72.0(3)°) are slightly more acute than those in **5** (vide supra). These geometric trends mirror those observed for base-free **1** and **2**. An even shorter Mn–Mn distance of 2.616(5) Å and a particularly acute Mn–C–Mn angle of 69.6(4)° were previously reported for isostructural [{MnCy(μ-Cy)}$_2$(μ-dmpe)] (Cy = cyclohexyl),[45] which features more sterically demanding and electron donating secondary alkyl groups.

Bright red X-ray-quality crystals of [{Mn(CH_2SiMe_3)(μ-CH_2SiMe_3)}$_2$(μ-dmpm)] (**7**) were obtained from hexanes at −30 °C (Figure 6), revealing a dimetallic structure analogous to the structures of the 2:1 MnR_2:dmpe complexes **5** and **6**. The

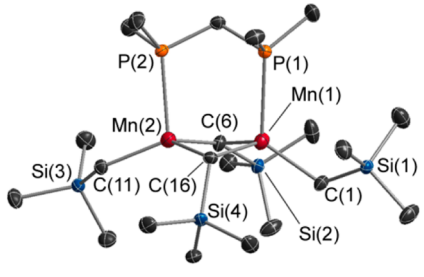

Figure 6. X-ray crystal structure for [{Mn(CH_2SiMe_3)(μ-CH_2SiMe_3)}$_2$(μ-dmpm)] (**7**). Hydrogen atoms are omitted for clarity, and ellipsoids are set to 50% (C, P, Si) and 70% probability (Mn). Bond distances (Å) and angles (deg): Mn(1)···Mn(2) 2.7243(5), Mn(1)–P(1) 2.6584(5), Mn(2)–P(2) 2.6016(6), Mn(1)–C(1) 2.134(1), Mn(2)–C(11) 2.121(1), Mn(1)–C(6) 2.220(2), Mn(2)–C(16) 2.233(1), Mn(1)–C(16) 2.340(1), Mn(2)–C(6) 2.337(1), Mn(1)–C(6)–Mn(2) 73.38(5), Mn(1)–C(16)–Mn(2) 73.08(4).

Mn–Mn, Mn–C, and Mn–P distances and Mn–C–Mn angles in **7** are very similar to those in **5**, although the dmpm ligand in **7** is bound less symmetrically than the dmpe ligand in **5** (the Mn–P distances in **7** differ by approximately 0.06 Å, in comparison with approximately 0.02 Å in **5**). The solid-state structure of [{Mn(CH_2CMe_3)(μ-CH_2CMe_3)}$_2$(μ-dmpm)] (**8**) was also determined using crystals obtained (a) from hexanes at −30 °C and (b) by slow evaporation of a hexanes solution at 20 °C (Figure S37 in the Supporting Information). However, the quality of both data sets was only suitable to establish connectivity, which is analogous to that of **7**.

The structures of **5** and **7** can also be compared with [{Mn(CH_2SiMe_3)(μ-CH_2SiMe_3)(PMe_3)}$_2$],[36a] and an isostructural PEt_3 complex, [{Mn(CH_2SiMe_3)(μ-CH_2SiMe_3)(PEt_3)}$_2$],[37] which was structurally characterized in this work (Figure S35 in the Supporting Information). Key differences are that the phosphine ligands in the PR_3 (R = Me, Et) complexes are trans to one another across the Mn–Mn axis, and the Mn–Mn distances (2.772(1) Å (R = Me) and 2.7937(3) Å (R = Et)) are 0.05–0.07 Å longer than those in **5** and **7**. Furthermore, the Mn–C–Mn angles in the monophosphine complexes (74.5(1)° for R = Me and 75.21(3)° for R = Et) are less acute than those in **5** and **7** (~73°), while Mn–P and Mn–C distances are comparable. These data highlight the substantial influence of the bidentate dmpe ligand on the relative orientation of the phosphorus donors, the Mn–Mn distance, and the Mn–C–Mn angle. The neopentyl complex [{Mn(CH_2CMe_3)(μ-CH_2CMe_3)(PMe_3)}$_2$][37] has also been reported, featuring an elongated Mn–Mn distance (2.718(3) Å) and statistically equivalent Mn–C–Mn angles (69.6(6)° and 71.0(6)°) relative to **6**.

NMR Spectroscopy and Magnetic Measurements. The ^{1}H NMR spectra of complexes **2**–**8** (Figure 7; C_6D_6, 500 MHz) show paramagnetically broadened and shifted peaks, between 5 and 60 ppm, with full width at half-maximum values from 1150 to 8200 Hz. Further spectra were collected in d_8-

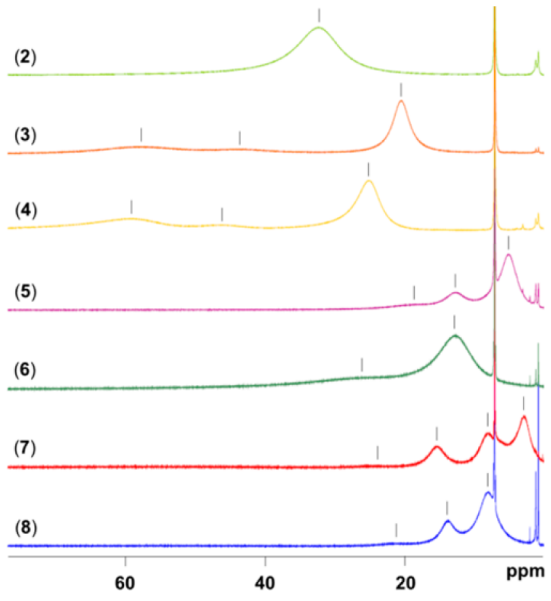

Figure 7. Room-temperature ^{1}H NMR spectra for **2**–**8** (500 MHz, C_6D_6). Black tick marks indicate broad peaks associated with organomanganese(II) complexes, while the sharp signals are due to residual C_6D_5H in the NMR solvent and trace hexanes.

DOI: 10.1021/acs.organomet.5b00907
Organometallics 2016, 35, 168–180

toluene between 186 K and room temperature (Figure 8 for **6**; Supporting Information for **2**–**5**, **7**, and **8**). A spectrum was not collected for **1** due to insolubility in noncoordinating solvents.

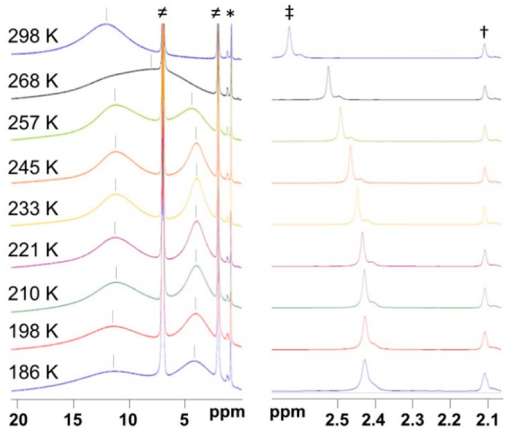

Figure 8. (left) ^{1}H NMR spectra for [{Mn(CH_2CMe_3)(μ-CH_2CMe_3)}$_2$(μ-dmpe)] (**6**) from 186 to 298 K (500 MHz, d_8-toluene). Broad signals (l) are due to **6**, while sharp signals are due to residual d_7-toluene solvent impurity (≠) and hexanes (*). (right) Region of the ^{1}H NMR spectra used for Evans measurements between 186 and 298 K (500 MHz, 40:1 d_8-toluene/toluene). The methyl group from external toluene (†) is calibrated to 2.11 ppm, and the methyl group of internal toluene (‡) is observed to shift with temperature. Shoulders to the right of the two toluene (C_7H_8) signals are the residual solvent signals due to d_7-toluene, $C_6D_5(CHD_2)$.

On the basis of the solid-state structure of phosphine-free **2**, six ^{1}H NMR signals are predicted with integrations of 36H, 18H, 18H, 8H, 4H, and 4H. However, it is not unreasonable to expect that the MnCH_2 signals would be broadened to the point at which they cannot be located, due to their proximity to the high-spin d^5 metal centers; in this case, a total of three ^{1}H NMR signals would be observed. At room temperature, the ^{1}H NMR spectrum of **2** shows only a single broad ^{1}H NMR resonance, but at −32 °C this peak splits into the expected three signals.

The ^{1}H NMR spectra for dmpe complexes **3** and **4**,[54] which do not contain bridging alkyl groups, would be expected to give rise to three signals (18H, 12H, and 4H, not including MnCH_2 signals), whereas the ^{1}H NMR spectra for **5**–**8** should give rise to four signals (18H, 18H, 12H, and 2H, not including MnCH_2 signals). The expected number of signals was observed for **3**, **4**, and **7** at 25 °C, below 10 °C for **5**, and below −28 °C for **8**. For compound **6**, just two ^{1}H NMR signals were observed at room temperature, and at −15 °C the largest of these signals split into two, yielding three broad peaks; the observation of just three signals (−15 to −80 °C) in the spectrum for **6** is likely due to coincidental overlap of two signals (Figure 8). The increased number of signals in the low-temperature ^{1}H NMR spectra of **2**, **5**, **6**, and **8** may be attributed to (a) different temperature dependencies for overlapping paramagnetically shifted signals or (b) decoalescence of signals that are averaged at room temperature due to exchange processes. For compound **8**, explanation (a) is most likely on the basis of solution magnetic measurements (vide infra). In contrast, for compounds **2**, **5**, and **6**, explanation (b) seems likely, given that solution magnetic measurements indicate that these tetrametallic or dimetallic complexes exist in equilibrium with other manganese-containing species in solution (vide infra).

Solid-state and solution magnetic measurements were carried out on complexes **2**–**8** (Table 1). SQUID magnetic measurements have previously been reported for **1** and show antiferromagnetic coupling/exchange between the manganese atoms.[39] SQUID magnetic measurements on **3**, which is monometallic, and **4**, which is a dimer with spatially separated manganese centers, show that both complexes obey the Curie–Weiss law (Figure 9; 300 to 5 K), leading to effective magnetic moments (μ_B) of 5.8 ± 0.2 and 5.83 ± 0.03 μ_B, respectively, and magnetic susceptibilities ($\chi_{M(corr)}$) of (14.0 ± 1.2) × 10^{-3} and (14.08 ± 0.13) × 10^{-3} cm^3/mol of Mn at room temperature (for a high-spin d^5 metal center, the ideal values for μ_B and χ_M(corr) are 5.92 μ_B and 14.6 × 10^{-3} cm^3/mol, respectively). Compounds **3** and **4** are therefore paramagnetic with no antiferromagnetic exchange.

Table 1. Room-Temperature Solution and Solid-State Magnetic Data for 2–8

	χ_M(corr) per Mn center[a] (10^{-3} cm^3/mol)	
complex	in C_6D_6 at 298 K	in the solid state at 300 K
2	4.2 ± 0.1[d]	2.82 ± 0.03
3	13.6 ± 0.5 (μ_B = 5.71 μ_B ± 0.11)[e]	14.0 ± 1.2 (μ_B = 5.8 μ_B ± 0.2)[b]
4	14.4 ± 0.5 (μ_B = 5.87 μ_B ± 0.10)	14.1 ± 0.1 (μ_B = 5.83 μ_B ± 0.03)[c]
5	3.5 ± 0.3	3.48 ± 0.04
6	6.5 ± 0.3	3.30 ± 0.03
7	3.0 ± 0.2	3.24 ± 0.03
8	3.4 ± 0.1	3.35 ± 0.03

[a] χM(corr) = corrected molar magnetic susceptibility; μ_B = effective magnetic moment; Θ = Weiss temperature. [b] Θ = −0.6 ± 0.1 K for **3**. [c] Θ = 0.04 ± 0.06 K for **4**. [d] Lit: 3.9 μ_B.[28b] [e] Lit: 5.6 μ_B.[36b]

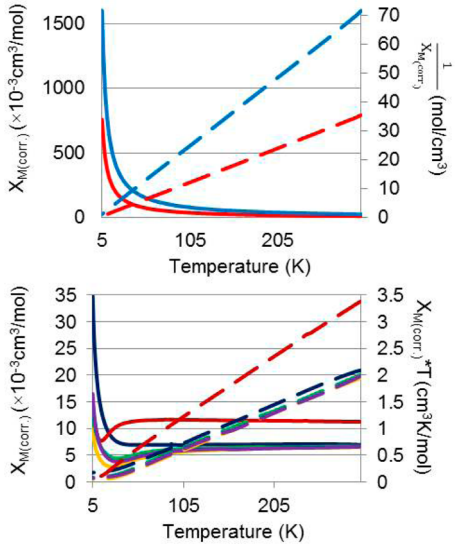

Figure 9. SQUID magnetic susceptibility data from 5 to 300 K: (top) χ_M(corr) vs T (solid lines) and (1/χ_M(corr)) vs T (dashed lines) for paramagnetic **3** (red) and **4** (blue); (bottom) χ_M(corr) vs T (solid lines) and [χ_M(corr)]T vs T (dashed lines) for **2** (red), **5** (blue), **6** (purple), **7** (orange), and **8** (green), which feature antiferromagnetic interactions.

In contrast, the SQUID magnetic data (Figure 9) for complexes **2** and **5**–**8**, which feature Mn–Mn distances

DOI: 10.1021/acs.organomet.5b00907
Organometallics 2016, 35, 168–180

between 2.685(1) and 2.7322(6) Å, do not obey the Curie law and are indicative of significant antiferromagnetic exchange/coupling between neighboring manganese centers (with paramagnetic impurity tails at low temperature). At room temperature, the magnetic susceptibility per manganese center is 2.82×10^{-3} cm^3/mol for tetrametallic **2** and ranges from 3.24×10^{-3} to 3.48×10^{-3} cm^3/mol for bimetallic **5**–**8**; these values are far lower than that expected for a paramagnetic metal center with five unpaired d electrons (14.6×10^{-3} cm^3/mol). The variable-temperature magnetic behavior of **2** and **5**–**8** is qualitatively similar to that reported for polymeric **1**[39] and dimetallic $[\{Mn(CH_2SiMe_3)_2(THF)\}_2]$,[42] and for the latter compound, Thompson et al. concluded that the significant magnetism observed at low temperatures indicates an absence of Mn–Mn bonding, despite the short Mn–Mn distance of 2.7878(9) Å.[42]

The SQUID magnetic susceptibility data for dinuclear **5**–**8** and tetranuclear **2** were fitted to an exchange expression (Supporting Information) for simple high-spin Mn(II) systems using MAGMUN-4.1,[55] and the resulting fits (Table 2 and Figures S29–S33 in the Supporting Information) are in good agreement with the experimental data. The resulting calculated g factors are close to 2.0, as expected for high-spin organomanganese(II) complexes which lack an orbital contribution to the magnetic moment, and the exchange coupling constants (J) for **2** and **5**–**8** range from −107 to −117 cm^{-1}, indicative of strong antiferromagnetic coupling (J is an averaged value for compound **2**).

Table 2. Magnetic Parameters Determined by Fitting an Exchange Expression to the SQUID Magnetic Susceptibility Data for Compounds 2 and 5–8[a]

compound[b]	mean g value	intradimer J (cm^{-1})	ρ	Θ (K)	100R
2[c]	2.07 ± 0.01	−117 ± 1	0.005	2.4	0.71
5	2.12 ± 0.02	−112 ± 2	0.02	4.9	1.47
6	2.10 ± 0.02	−112 ± 2	0.01	1.1	1.03
7	2.07 ± 0.01	−109 ± 1	0.007	3.4	0.82
8	2.04 ± 0.03	−107 ± 2	0.011	5.1	1.06

[a] J = exchange coupling constant; ρ = fraction paramagnetic impurity; Θ = Weiss-like temperature correction; $R = [(\sum\chi_{obs} - \chi_{calc})^2/(\sum\chi_{obs})^2]^{1/2}$. [b] The calculated temperature independent paramagnetism (TIP) is 0 cm^3/mol for **2**, **6**, and **7**, 4×10^{-5} cm^3/mol for **5**, and 3×10^{-5} cm^3/mol for **8**. [c] For **2**, J is an average over the three Mn–Mn interactions present.

Solution-state magnetic measurements were conducted using the Evans NMR method (Figure 8 and Supporting Information).[56] Measurements were taken at room temperature for all complexes (in a 40:1 C_6D_6/C_6H_6 mixture) and between 298 and 186 K for **2** and **5**–**7** (in a 40:1 d_8-toluene/toluene mixture). Complexes **3** and **4**, which are monometallic or feature well-separated manganese centers, have room-temperature solution effective magnetic moments of 5.71 and 5.87 μ_B, respectively, which are very close to the theoretical value of 5.92 μ_B and are statistically equivalent to the solid-state effective magnetic moments. dmpm complexes **7** and **8** gave rise to statistically identical solution and solid-state magnetic susceptibilities at room temperature, indicating that the solid-state structures of **7** and **8** remain intact in solution. Additionally, variable-temperature Evans magnetic measurements on compound **7** (Figure 10; 298 to 186 K) yielded magnetic susceptibility values that are statistically equivalent to those from SQUID measurements over the same temperature range.

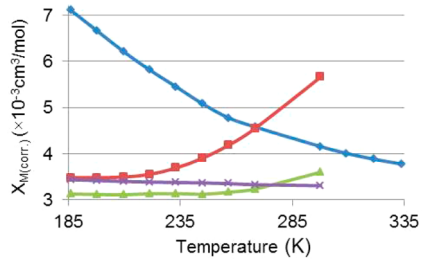

Figure 10. Solution magnetic susceptibilities per mole of Mn calculated from Evans measurements at various temperatures for $[\{Mn(CH_2CMe_3)(\mu\text{-}CH_2CMe_3)_2\}_2\{Mn(\mu\text{-}CH_2CMe_3)_2Mn\}]$ (**2**) (blue ♦), $[\{Mn(CH_2SiMe_3)(\mu\text{-}CH_2SiMe_3)\}_2(\mu\text{-dmpe})]$ (**5**) (green ▲), $[\{Mn(CH_2CMe_3)(\mu\text{-}CH_2CMe_3)\}_2(\mu\text{-dmpe})]$ (**6**) (red ■), and $[\{Mn(CH_2SiMe_3)(\mu\text{-}CH_2SiMe_3)\}_2(\mu\text{-dmpm})]$ (**7**) (purple ×).

In contrast, the solution magnetic susceptibilities for base-free **2** and dimetallic **6** are significantly higher than the solid-state values (although they are still much lower than those expected in the absence of antiferromagnetic exchange). For dimetallic **6**, the solution magnetic susceptibility values decreased as the temperature was lowered, until an asymptote was reached at a value corresponding to that from solid-state SQUID measurements; compound **5** showed analogous behavior, but with a much less pronounced change in magnetic susceptibility (Figures 9 and 10). This behavior is consistent with a solution equilibrium (significant above 245 K for **5** and above 210 K for **6**) between the dimetallic solid-state structures and entropically favored paramagnetic species; most likely mononuclear $[Mn(CH_2EMe_3)_2(dmpe)]$ (E = Si (**3**), C (**4**)) and base-free "$Mn(CH_2EMe_3)_2$". Our inability to directly observe the proposed minor solution species by variable-temperature ^{1}H NMR spectroscopy is consistent with the low concentrations of these species in solution, the broadness of the observed ^{1}H NMR signals, and the likelihood of rapid exchange between these species and **5** and **6**, especially at the upper end of the temperature range.

Unlike the solution magnetic susceptibility data for complexes **5** and **6**, the solution magnetic susceptibility of base-free **2** increased as the temperature was reduced and did not reach a plateau (Figure 10), moving increasingly further from the solid-state magnetic susceptibility value of 2.82×10^{-3} cm^3/mol of Mn. This increase in magnetic susceptibility is indicative of an equilibrium that shifts at lower temperature toward species with weaker antiferromagnetic coupling in comparison to that observed in tetrametallic **2**. Above room temperature, the magnetic susceptibility of the solution (per manganese atom) continued to decrease toward the solid-state value, but magnetic measurements were not accessible above 60 °C ($\chi_M(corr) = 3.8 \times 10^{-3}$ cm^3/mol) due to slow decomposition of solutions of **2** above this temperature.

Physical Properties of 1–8. Melting points ranging from 62 to 176 °C were measured for **1**–**8** in a flame-sealed glass capillary under an atmosphere of argon (Table 3). All complexes were found to melt without noticeable decomposition (determined visually and by ^{1}H NMR spectroscopy and/or PXRD after cooling to room temperature) if the temperature was reached quickly (5 °C/min), with the exception of **6**, which showed minor decomposition.

DOI: 10.1021/acs.organomet.5b00907
Organometallics 2016, 35, 168–180

Table 3. Physical Properties of Complexes 1−8

complex	mp (°C)	sublimation temp at 5 mTorr (°C)	thermal dec data (°C)[a]
1	151−153 (lit. 98)[28b]	150−160 (lit. 150)[39]	195 (rapid dec)
2	99−102	90 (lit. 100)[28b]	110 (>50% after 24 h)
3	62−63 (lit. 62−64)[36b]	60	120 (v. little over 24 h)
4	132 (lit. 132−133)[36b]	80	120 (complete after 5−6 h)
5	145−146	115−135 (dec products sublime)	120 (complete after 5−6 h)
6	149−151.5 (partial dec)	110	110 (visible after 2−3 h)
7	176	100	120 (very little over 24 h)
8	161.5−165	100−120	110 (very little over 24 h)

[a]Amount of decomposition assessed visually and by ^{1}H NMR spectroscopy and/or PXRD after cooling to room temperature.

Importantly, the melting points of **3** and **4** match those reported by Wilkinson et al.,[36b] confirming that the originally reported complexes were 1:1 Mn/dmpe complexes as proposed, rather than 2:1 complexes.

Base-free $[\{Mn(\mu\text{-}CH_2SiMe_3)_2\}_\infty]$ (**1**), though very thermally stable (rapid decomposition at 195 °C), is not especially volatile (sublimation at 150−160 °C; 5 mTorr). This low volatility can be explained by the polymeric nature of **1** in the solid state. In contrast, $[\{Mn(CH_2CMe_3)(\mu\text{-}CH_2CMe_3)_2\}\{Mn(\mu\text{-}CH_2CMe_3)_2Mn\}]$ (**2**), which exists as a monomer in the vapor phase,[47] sublimed at 90 °C (5 mTorr) but was more than 50% decomposed after 24 h at 110 °C. The remaining complexes, **3**−**8**, sublimed between 60 and 135 °C at 5 mTorr, although **5** underwent extensive decomposition during sublimation and **6** and **8** decomposed slowly at the sublimation temperature (Table 3). The 1:1 MnR_2/dmpe complexes, monometallic **3** and dimetallic **4**, exhibited the most promising volatility/thermal stability characteristics for possible applications in ALD or CVD, subliming at 60 and 80 °C, respectively, with negligible decomposition after 24 h at 120 and 110 °C, respectively. Furthermore, **3** has a melting point of 62−63 °C and thus would be a liquid at the delivery temperature in a typical ALD or CVD experiment.

Reactions with Hydrogen and Diethylzinc. Solutions of complexes **2**−**8**, or a slurry of **1**, were placed under 2 atm of H_2 in an aromatic solvent, the reactions were monitored by ^{1}H NMR spectroscopy (Figures S46−S55 in the Supporting Information), and insoluble products were characterized using PXRD (Figures S64−S65 in the Supporting Information). Reactions took place between 25 and 120 °C (Table 4), and in each case, a clear colorless or very pale beige solution was formed with a metallic-looking silver-gray mirror on the walls of the NMR tube (Scheme 3), or in one case (complex **1**) a precipitate of black powder. The diamagnetic reaction byproducts were tetramethylsilane or neopentane, accompanied by dmpe or dmpm in the case of compounds **3**−**8** (Scheme 3). The deposited solid was identified as manganese metal by PXRD. Additionally, conducting the reactions of **3** and **5** with H_2 in the presence of hexaethylbenzene as an internal NMR standard yielded exactly 2 and 4 equiv of $SiMe_4$, respectively,[57] illustrating complete removal of the alkyl groups from manganese. The appearance of the deposited films is also consistent with metallic manganese.

Polymeric complex **1** was the least reactive toward hydrogen, requiring several days at 120 °C to react completely, most likely due to very low solubility. In contrast, highly soluble tetrametallic **2** reacted to completion within 3 days at room temperature; **2** is far more reactive than **1** and **3**−**8**, likely due to the presence of three-coordinate manganese centers. Complexes **3** and **4**, which contain 1 equiv of dmpe per manganese center, showed low reactivity toward H_2; the reaction with **3** was only complete after 12 h at 120 °C, and the reaction with **4** was complete after 24 h at 100 °C. Dimetallic **5** and **6**, which contain 1/2 equiv of dmpe per manganese center, reacted with H_2 to form **3** or **4**, accompanied by tetramethylsilane or neopentane and manganese metal. Complete consumption of **5** required 4.5 h at 120 °C,[58] and the analogous reaction with **6** proceeded over 1 week at room temperature. The similarity in the reaction conditions required for consumption of **6** and **2** supports the proposal (vide supra) that, in solution, **6** exists in equilibrium with **2** and **4** (i.e., H_2 likely reacts with **2** that is in equilibrium with **6** in solution, leaving unreacted **4**). Compounds **7** and **8** reacted with H_2 over the course of 4 h at 120 and 100 °C, respectively. However, unlike the dmpe analogues (**5** and **6**), compounds **7** and **8** reacted with H_2 to provide manganese metal without formation of an observable monometallic intermediate. A general trend for **1**−**8** is the greater reactivity of the neopentyl complexes toward H_2.

Overall, the reactions of the dialkylmanganese(II) complexes and their bisphosphine adducts with H_2 highlight the utility of

Table 4. Reaction Conditions and Byproducts for (i) the Solution Reactions of 1−8 with H_2 Yielding Mn Metal (Determined by PXRD) and (ii) Solution Reactions of 1−8 with $ZnEt_2$ To Deposit a 1:1 Mn/Zn Alloy (Determined by PXRD and in Some Cases XPS; Accompanied by Zn Metal Deposition in the Reaction of 2 with $ZnEt_2$)

complex	$T_{reaction}$ with H_2 (°C)/time (h)	H_2 reaction byproducts[b]	$T_{reaction}$ with $ZnEt_2$ (°C)/time (h)	$ZnEt_2$ reaction byproducts[a,b]
1	120/48	$SiMe_4$	25/12	C_2H_6, C_2H_4, $SiMe_4$, ZnRX
2	25/72	CMe_4	25/12	C_2H_6, C_2H_4, CMe_4, ZnRX
3	120/24	$SiMe_4$, dmpe	60/1	C_2H_6, C_2H_4, **9**,[d] $SiMe_4$, u.p.[c]
4	70/216 (or 100/24)	CMe_4, dmpe	25/72	C_2H_6, C_2H_4, **9**,[d] ZnRX
5	120/4	$SiMe_4$, **3**	25/48	C_2H_6, C_2H_4, **9**,[d] $SiMe_4$, ZnRX,
6	25/168 (or 60/1)	CMe_4, **4**	25/12	C_2H_6, C_2H_4, **9**,[d] ZnRX, u.p.[c]
7	120/4	$SiMe_4$, dmpm, u.p.[c]	90/0.5	C_2H_6, C_2H_4, ZnRX, dmpm
8	100/4	CMe_4, dmpm	95/1	C_2H_6, C_2H_4, ZnRX, dmpm

[a]R = CH_2EMe_3; X = Et, R; E = C, Si. [b]Byproducts identified by ^{1}H NMR spectroscopy. [c]u.p. = unidentified product. [d]Compound **9** is $[MnH(C_2H_4)(dmpe)_2]$.[60]

DOI: 10.1021/acs.organomet.5b00907
Organometallics 2016, 35, 168−180

Scheme 3. Reactions of 1−8 with H_2 in Benzene or Toluene

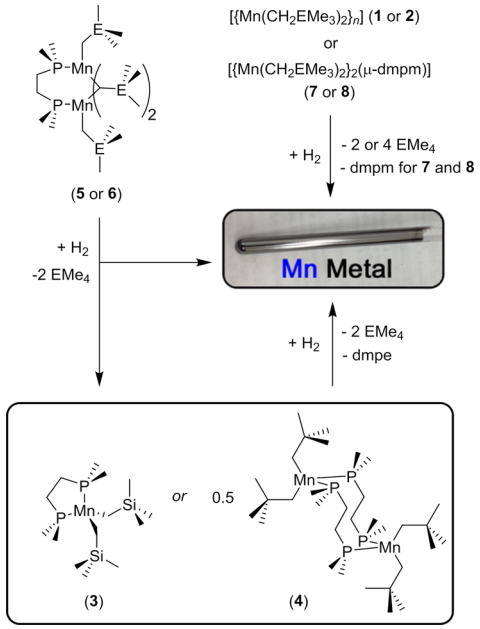

metal alkyl complexes for electropositive metal deposition, demonstrating the thermodynamic feasibility of key reaction steps en route to manganese deposition. In solution, base-free **2** and dmpe complex **6** displayed the highest reactivity. However, solution reaction temperatures may not be of direct relevance to thermal ALD, given that adsorption to the surface of the growing thin film during ALD is likely to result in phosphine dissociation and/or formation of surface-bound species with coordination geometries and steric environments which differ significantly from those in the intact precursor complex.

Complexes **1**−**8** were also reacted with 1−3 equiv of $ZnEt_2$ (per Mn) in C_6D_6 (**2**-**8**) or d_8-toluene (**1**) in a sealed NMR tube; the reactions were monitored by ^1H and/or ^{31}P NMR spectroscopy (Figures S56−S63 in the Supporting Information), and precipitated solids were characterized by PXRD and in some cases XPS (Figures S66−S71 in Supporting Information). Complexes **1**, **2**, and **4**−**6** reacted completely over 12−72 h at room temperature, whereas **3** required heating for 1 h at 60 °C and dmpm complexes **7** and **8** required heating at 90−95 °C for 30−60 min. In each of these reactions, a silver-colored mirror was deposited onto the walls of the NMR tube, and ethane, ethylene, and $ZnX(CH_2EMe_3)$ (X = Et, CH_2EMe_3; E = Si, C) were released, accompanied in some cases by a small amount of EMe_4 (E = Si, C); H_2 formation was not observed. Compounds **7** and **8** released free dmpm,[59] whereas dmpe compounds **3**−**6** formed $[MnH(C_2H_4)(dmpe)_2]$ (**9**)[60] (0.5 equiv per Mn in **3** and **4** and 0.25 equiv per Mn in **5** and **6**; Scheme 4), and free dmpe was not liberated.

Scheme 4. Reactions of Dmpe Complexes 3−6 with $ZnEt_2$ (R = CH_2EMe_3; X = Et, R; E = C, Si) in Benzene

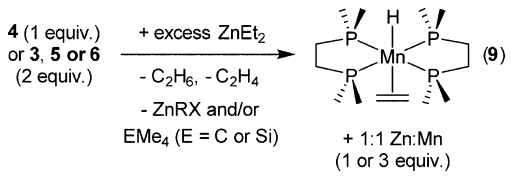

The reactivities of **5** and **6** with $ZnEt_2$ are greater than those of **3** and **4**, respectively, implying that **3** and **4** are not formed as intermediates in the reactions of **5** and **6** with $ZnEt_2$, in contrast to the analogous reactions with H_2 (vide supra). The aforementioned manganese(I) hydride compound, diamagnetic $[MnH(C_2H_4)(dmpe)_2]$ (**9**), was first prepared by Wilkinson et al. via the reactions of manganese dihalides with $MgEt_2$[45] and may be formed in this work by bimolecular HR reductive elimination from manganese dihydride and manganese hydrido/alkyl centers or comproportionation between a manganese dihydride species and elemental manganese (or an unobserved zerovalent manganese species formed en route to manganese metal).

By PXRD, the insoluble product from the reactions of **1**−**8** with $ZnEt_2$ was a 1:1 manganese/zinc alloy,[61] accompanied by zinc metal in the case of **2**. The presence of both zinc and manganese was further confirmed by XPS on representative samples (Zn/Mn = 0.68:1 for **2** and 1.32:1 for **7**). Elemental zinc deposition could potentially occur via hydride transfer from a manganese hydride intermediate to a dialkyl zinc compound, leading to a zinc hydrido/alkyl species with very limited thermal stability; the only isolated zinc hydrido hydrocarbyl compounds contain extremely large aryl groups (e.g. R = C_6H_3-2,6-(C_6H_3-2,6-iPr$_2$)$_2$,[62] C_6H_3-2,6-(C_6H_2-2,4,6-iPr$_3$)$_2$, C_6H_2-2,6-(C_6H_2-2,4,6-iPr$_3$)$_2$-4-SiMe$_3$)[63]), although ZnHMe has been observed in an argon matrix[64] and by spectroscopy in the gas phase.[65,66]

SUMMARY AND CONCLUSION

In the solid state, dineopentylmanganese(II) (**2**) is tetrametallic with two terminal alkyl groups and six bridging alkyl groups. The outer manganese centers are trigonal planar, whereas the inner manganese centers are tetrahedral. dmpe complexes of bis(trimethylsilylmethyl)manganese(II) and dineopentylmanganese(II) adopt three distinct structural types: monometallic $[LMnR_2]$ (**3**), dimetallic $[R_2Mn(\mu\text{-}L)_2MnR_2]$ (**4**), and dimetallic $[\{RMn(\mu\text{-}R)\}_2(\mu\text{-}L)]$ (**5** and **6**). In contrast, dmpm only yielded $[\{RMn(\mu\text{-}R)\}_2(\mu\text{-}L)]$ complexes (**7** and **8**). All polymetallic complexes with doubly bridging alkyl groups feature one long and one short Mn−C bond, and the neopentyl complexes exhibit more acute Mn−C−Mn angles and shorter Mn−Mn distances than trimethylsilylmethyl analogues.

All complexes have nonzero magnetic susceptibilities between 300 and 5 K. Both $[Mn(CH_2SiMe_3)_2(dmpe)]$ (**3**) and $[\{Mn\text{-}(CH_2CMe_3)_2(\mu\text{-dmpe})\}_2]$ (**4**) obey the Curie−Weiss law, whereas tetrametallic dineopentylmanganese(II) (**2**) and $[\{RMn(\mu\text{-}R)\}_2(\mu\text{-}L)]$ (L = dmpe (**5** and **6**), dmpm (**7** and **8**)) engage in strong antiferromagnetic coupling with J values from −107 to −117 cm^{-1}. A comparison of solution and solid-state magnetic data indicates that the structures of the dmpm complexes (**7** and **8**) are maintained in solution, whereas the $[\{RMn(\mu\text{-}R)\}_2(\mu\text{-dmpe})]$ complexes (**5** and **6**) exist in equilibrium at 25 °C with species with a higher average magnetic susceptibility: most likely $[(dmpe)MnR_2]$ and "MnR_2". However, the solution magnetic susceptibilities of **5** and **6** decreased with decreasing temperature until an asymptote was reached, consistent with the presence of only **5** or **6** in solution at low temperature. In contrast, the magnetic susceptibility (per Mn) of dineopentylmanganese(II) (**2**) almost doubled as the temperature was reduced from 335 to 185 K, implying that the tetrametallic solid-state structure is in

DOI: 10.1021/acs.organomet.5b00907
Organometallics 2016, 35, 168−180

equilibrium with species which exhibit less effective antiferromagnetic coupling and are favored at lower temperatures.

The two compounds without bridging alkyl groups (**3** and **4**) exhibited the most desirable thermal stability and volatility for ALD or CVD applications, and all CH_2SiMe_3 derivatives exhibited slightly increased thermal stability relative to CH_2CMe_3 analogues; monometallic **3** was the most promising, melting at 62−63 °C, subliming at 60 °C (5 mTorr), and undergoing negligible decomposition after 24 h at 120 °C.

Solution reactions of **1**−**8** with H_2 yielded manganese metal with elimination of 2 equiv of HR (R = CH_2EMe_3; in all cases, neopentyl complexes displayed higher reactivity toward H_2 than trimethylsilylmethyl analogues), demonstrating the thermodynamic feasibility of the key reaction steps required for manganese(II) dialkyl complexes to serve, in combination with H_2, as precursors for metal ALD or pulsed CVD. In contrast, the solution reactions of **1**−**8** with $ZnEt_2$ yielded a zinc/manganese alloy with an approximate 1:1 Zn/Mn ratio, eliminating ethane and ethylene, accompanied by dmpm, $[MnH(C_2H_4)(dmpe)_2]$ (**9**), EMe_4, and/or ZnXR (R = CH_2EMe_3; X = Et, R). ALD/pulsed CVD studies using **3**, **4**, and the recently reported $[(allyl^{TMS2})Mn\{C(SiMe_3)_3\}(PMe_3)]$[67] in combination with H_2 are in progress and will be reported in due course.

EXPERIMENTAL SECTION

General Details. An argon-filled MBraun UNIlab glovebox equipped with a −30 °C freezer was employed for the manipulation and storage of all oxygen- and moisture-sensitive compounds. Air-sensitive preparative reactions were performed on a double-manifold high-vacuum line equipped with a two-stage Welch 1402 belt-drive vacuum pump (ultimate pressure 1×10^{-4} Torr) using standard techniques.[68] The vacuum was measured periodically using a Kurt J. Lesker 275i convection enhanced Pirani gauge, and residual oxygen and moisture were removed from the argon stream by passage through an Oxisorb-W scrubber from Matheson Gas Products. Commonly utilized specialty glassware included a swivel frit assembly, thick-walled flasks equipped with Teflon stopcocks, J. Young or Wilmad-LabGlass LPV NMR tubes, Wilmad-LabGlass LPV EPR tubes, and Starna 1-Q-10/GS UV−vis−NIR cells with Spectrosil far-UV quartz windows (transparent from 170 to 2700 nm), quartz to Pyrex graded seals, and Teflon stopcocks. Where indicated, a Branson 2510 ultrasonic bath was used to sonicate reaction mixtures. A VWR Clinical 200 Large Capacity Centrifuge (with 28° fixed-angle rotors that hold 12 × 15 mL or 6 × 50 mL tubes, in combination with VWR high-performance polypropylene conical centrifuge tubes) located within a glovebox was used where indicated.

Anhydrous diethyl ether was purchased from Aldrich, hexanes and toluene were purchased from Caledon, and deuterated solvents were purchased from ACP Chemicals. Hexanes and toluene were initially dried and distilled at atmospheric pressure from sodium/benzophenone and sodium, respectively. All solvents were stored over an appropriate drying agent (diethyl ether, toluene, d_8-toluene, C_6D_6 = Na/Ph_2CO; hexanes = Na/Ph_2CO/tetraglyme) and introduced to reactions or solvent storage flasks via vacuum transfer with condensation at −78 °C.

dmpe, dmpm, trimethylsilylmethylmagnesium chloride solution (1.0 M in diethyl ether), and 1,4-dioxane were purchased from Sigma-Aldrich. Manganese dichloride, neopentyl chloride, and diethylzinc (minimum 95% in a Sure-Pak cylinder) were purchased from Strem Chemicals. Argon and hydrogen gas were purchased from PraxAir. Bis(trimethylsilylmethyl)magnesium[69] and dineopentylmagnesium[28b] were prepared according to the literature, though a slight excess of 1,4-dioxane was used, leading to between 0.25 (trimethylsilylmethyl) and 0.8 equiv (neopentyl) of 1,4-dioxane in the products. Bis(trimethylsilylmethyl)manganese(II)[39] was prepared according to literature procedures, though the reactant bis(trimethylsilylmethyl) magnesium contained 0.25 equiv of 1,4-dioxane. $[\{Mn(CH_2SiMe_3)(\mu\text{-}CH_2SiMe_3)(PEt_3)\}_2]$ was prepared as previously described.[37]

NMR spectroscopy (^1H, ^{13}C, and $^{31}P\{^1H\}$) was performed on Bruker DRX-500, AV-200, and AV-600 spectrometers. Spectra were obtained at 298 K unless otherwise indicated. All ^1H NMR spectra were referenced relative to $SiMe_4$ through a resonance of the proteo impurity of the solvent used: C_6D_6 (δ 7.16 ppm) and toluene-d_8 (δ 2.08, 6.97, 7.01, and 7.09 ppm). In addition, all ^{13}C NMR spectra were referenced relative to $SiMe_4$ through a resonance of the trace ^{13}C in the solvents: C_6D_6 (δ 128.06 ppm) and toluene-d_8 (δ 20.43, 125.13, 127.96, 128.87, and 137.48 ppm). The ^{31}P NMR spectra were referenced using an external standard of 85% H_3PO_4 in D_2O (0.0 ppm). Various impurities (normally solvents) were identified by comparing to the tables of NMR chemical shifts of common impurities prepared by Goldberg et al.[70] Evans NMR measurements were conducted on the Bruker DRX-500 spectrometer in a manner described in the Supporting Information, and values are the average of two independent experiments. For **2**, χ_M(corr) values above and below room temperature were collected using two different sets of samples; the values from 298 to 335 K were adjusted to give the same room-temperature value by correcting the mass used from 8.3 to 8.6 mg, which is within the error of the mass balance.

Combustion elemental analyses were performed on a Thermo EA1112 CHNS/O analyzer. Samples for elemental analysis (typically 1−4 mg) were packed and sealed in preweighed 3 × 6 mm smooth wall tin capsules inside the glovebox. After removal from the glovebox, these capsules were packed into 5 × 8 mm pressed aluminum capsules containing approximately 10 mg of V_2O_5.

Single-crystal X-ray crystallographic analyses were performed on crystals coated in Paratone oil and mounted on a SMART APEX II diffractometer with a 3 kW sealed-tube Mo generator and SMART6000 CCD detector in the McMaster Analytical X-ray (MAX) Diffraction Facility. Numerical absorption corrections were applied by face indexing, and a further semiempirical absorption correction was applied using redundant data. Raw data were processed using XPREP (as part of the APEX v2.2.0 software) and solved by direct methods (SHELXS-97).[71] The structure was completed by difference Fourier synthesis and refined with full-matrix least-squares procedures based on F^2. In all cases, non-hydrogen atoms were refined anisotropically and hydrogen atoms were generated in ideal positions and then updated with each cycle of refinement. Powder X-ray diffraction experiments were performed on a Bruker D8 Advance powder diffractometer with Cu Kα radiation (λ = 0.154 nm) operated at 40 kV and 40 mA. Powders were packed in 0.5 mm o.d. special glass (SG; wall thickness 0.01 mm) capillary tubes for X-ray diffraction (purchased from Charles Supper Co.) and sealed by inverting to submerge the open end in a pool of Apiezon H-grease within the glovebox. Calculated powder patterns were generated from the low-temperature single-crystal data (for complexes **2**−**8**) and a file downloaded from the Cambridge Crystallographic Database (for complex **1**)[39] using Mercury. Experimental powder diffractograms were generated and viewed using Gadds, Powdercell, Crystal Sleuth, Diffrac.eva, Topaz, and PANalytical HighScore.

UV/vis spectra were obtained on a Cary 50 UV/visible spectrometer using 10 mM to 10 μM solutions in hexanes. Melting points were measured on a DigiMelt SRS MPA 160 melting point apparatus; between 1 and 2 mg of each sample was flame-sealed in a thin glass tube under an atmosphere of argon. X-ray photoelectron spectra were collected on either a Thermo Scientific Thetaprobe or a K-Alpha instrument (Thermo Scientific, East Grinstead, U.K.), both of which are located at the University of Toronto. A monochromated Al K-Alpha was used with a spot size of 400 μm. An initial survey spectrum was collected at low-energy resolution for composition, as well as the high-energy resolution spectrum of the Zn 2p, Zn Aug, and Mn 2p regions. SQUID measurements were collected on a Quantum Design MPMS instrument between 5 and 300 K at applied fields ranging from 100 Oe (for most) to 10000 Oe (for complexes **3** and **6**). Roughly 50 mg of sample was placed in a sealed sample rod assembly for transport of air-sensitive samples into the magnetometer (with the

DOI: 10.1021/acs.organomet.5b00907
Organometallics 2016, 35, 168−180

exception of **3**, where between 2.9 and 3.4 mg of sample was placed in a flame-sealed glass capillary).

Thermal stability data were obtained by sealing approximately 10 mg of powder under argon in a flask with a Teflon valve. This flask was heated to the desired temperature for 24 h and then cooled to room temperature for visual inspection as well as PXRD and/or ^{1}H NMR spectroscopy. When "very little" is used to describe the extent of decomposition, this indicates that the compound darkened in color but that decomposition was not observed by PXRD or ^{1}H NMR spectroscopy.

Complexes **1**−**8** are exceptionally air sensitive, as is diethylzinc, and the phosphines dmpm and dmpe are malodorous. Therefore, all syntheses were conducted under an atmosphere of argon, in a fume hood where necessary.

[{Mn(CH$_2$CMe$_3$)(μ-CH$_2$CMe$_3$)$_2$}$_2${Mn(μ-CH$_2$CMe$_3$)$_2$Mn}] (2). $MnCl_2$ (2 g, 15.9 mmol) was suspended in 20 mL of diethyl ether. $Mg(CH_2CMe_3)_2(1,4\text{-dioxane})_{0.8}$ (4.9 g, 20.7 mmol) was dissolved separately in 40 mL of diethyl either and added dropwise to the $MnCl_2$ suspension over 20 min. The reaction was stirred at room temperature for 4 days with regular sonication. The resulting yellow/light brown suspension was centrifuged to remove $MgCl_2$, and the solvent was removed from the resulting solution in vacuo. Crude **2** was extracted into toluene, forming a dark brown solution, and the solvent was again removed in vacuo. The remaining solid was recrystallized from hexanes (∼10 mL) at −30 °C to afford large brown crystals. The mother liquors were then concentrated and maintained for several days at −30 °C to afford a second batch of crystals; the total yield was 60% (1.88 g). Note that, on one occasion, a white solid was obtained rather than the expected dark brown solid. This solid was likely the Et_2O or 1,4-dioxane adduct of dineopentylmanganese(II) and was converted to pure **2** by extended exposure to dynamic vacuum. Compound **2** was found to sublime at 90 °C (5 mTorr) and to melt between 99 and 102 °C. X-ray-quality crystals were obtained from hexanes at −30 °C. ^{1}H NMR: (C_6D_6) 32.6 ppm; (d_8-toluene, 298 K) 28.2; (d_8-toluene, 233 K) 14.9, 28.9, 65.9 ppm. Vis: λ_{max} 464 nm. Anal. Found (calcd): C, 60.18 (60.90); H, 10.75 (11.24).

[Mn(CH$_2$SiMe$_3$)$_2$(dmpe)] (3) and [{Mn(CH$_2$CMe$_3$)$_2$(μ-dmpe)}$_2$] (4). The 1:1 dialkylmanganese(II)/dmpe adducts were prepared according to literature procedures.[36b] Complex **3** was purified by sublimation (60 °C at 5 mTorr) to give a bright yellow powder, and complex **4** was purified by recrystallization from hexanes to afford a white powder (**4** also sublimed cleanly between 80 and 100 °C at 5 mTorr). X-ray-quality crystals of **3** and **4** were obtained from hexanes at −30 °C. Data for complex **3** are as follows. ^{1}H NMR: (C_6D_6) 20.6, 44.0, 58.1 ppm; (d_8-toluene, 298 K) 20.6, 43.4, 56.4 ppm; (d_8-toluene, 233 K) 26.2, 76 (v broad) ppm. Anal. Found (calcd): C, 44.16 (44.31); H, 10.36 (10.09). Data for complex **4** are as follows. ^{1}H NMR: (C_6D_6) 25.2, 46.3, 59.1 ppm; (d_8-toluene, 298 K) 25.1, 45.6, 56.5 ppm; (d_8-toluene, 233 K) 30.6, 67 (v broad) ppm. Anal. Found (calcd): C, 56.02 (55.32); H, 11.11 (11.03).

[{Mn(CH$_2$SiMe$_3$)(μ-CH$_2$SiMe$_3$)$_2$}$_2$(dmpe)] (5). [{Mn(μ-$CH_2SiMe_3)_2$}$_\infty$] (**1**; 67.1 mg, 0.294 mmol of Mn) and [Mn-$(CH_2SiMe_3)_2$(dmpe)] (**3**; 110.9 mg, 0.292 mmol) were dissolved in toluene at −78 °C. The resulting light orange solution was stirred for 1 h at −78 °C and 3 h at room temperature before solvent was removed in vacuo. The resulting powder was dissolved in 1 mL of hexanes, centrifuged to remove a white solid impurity, and maintained at −30 °C for several days to produce orange-red crystals, which when crushed yielded an orange powder (87.2 mg; 49% yield). The product was found to melt cleanly between 145 and 146 °C when heated quickly. ^{1}H NMR: (C_6D_6) 5.2, 12.7, 19 (v broad) ppm; (d_8-toluene, 298 K) 5.2, 12.7, 19 (v broad) ppm; (d_8-toluene, 233 K) 2.5, 7.6, 12.1, 19 (v broad) ppm. Vis: λ_{max} 477 nm. Anal. Found (calcd): C, 43.01 (43.40); H, 9.58 (9.93).

[{Mn(CH$_2$CMe$_3$)(μ-CH$_2$CMe$_3$)}$_2$(μ-dmpe)] (6). Tetrametallic **2** (110 mg, 0.14 mmol) and dimetallic **4** (200 mg, 0.29 mmol) were dissolved in 5 mL of toluene. The solution was stirred overnight at room temperature and then maintained at −30 °C for several days to obtain black crystals. The mother liquor was concentrated and maintained at −30 °C for several days to obtain a second batch of crystals, leading to a total yield of 92% (279 mg). The product sublimed at 110 °C at 5 mTorr and melted with some decomposition between 149 and 151.5 °C. ^{1}H NMR: (C_6D_6) 12.8, 26 (v broad) ppm; (d_8-toluene, 298 K) 12.2, 25 (v broad) ppm; (d_8-toluene, 233 K) 4.0, 11.3, 31 (v broad) ppm. Vis: λ_{max} 486 nm. Anal. Found (calcd): C, 57.06 (57.34); H, 11.23 (11.11).

[{Mn(CH$_2$SiMe$_3$)(μ-CH$_2$SiMe$_3$)}$_2$(dmpm)] (7). A suspension of [{Mn(μ-$CH_2SiMe_3)_2$}$_\infty$] (**1**; 119 mg, 0.52 mmol per Mn) in toluene (20 mL) was cooled to −78 °C. A solution of dmpm (180 mg, 1.3 mmol) in toluene (2 mL) was then added dropwise, and after the suspension was stirred for 30 min at −78 °C and 1.5 h at room temperature, it turned to a clear orange solution. The solvent was then removed in vacuo, and the solid was extracted with hexanes. After the extract was centrifuged to remove residual solid, the clear red hexanes solution was maintained at −30 °C for several days. The resulting red crystals were of X-ray quality. Crushing the crystals afforded a light pink powder (99 mg; 52% yield). Complex **7** sublimed cleanly at 100 °C (5 mTorr) and melted without significant decomposition when heated rapidly to 176 °C (note: partial melting commenced at 160 °C). ^{1}H NMR: (C_6D_6) 3.1, 7.9, 15.5, 24 (v broad) ppm; (d_8-toluene, 298 K) 3.1, 7.7, 15.4, 25 (v broad) ppm; (d_8-toluene, 233 K) 2.5, 8.4, 15.4, 25 (v broad) ppm. Vis: λ_{max} 476 nm. Anal. Found (calcd): C, 42.24 (42.40); H, 9.86 (9.83).

[{Mn(CH$_2$CMe$_3$)(μ-CH$_2$CMe$_3$)}$_2$(dmpm)] (8). dmpm (220 mg, 1.61 mmol) was added to a solution of tetrametallic **2** (310 mg, 0.39 mmol) in a 4:1 mixture of hexanes and toluene (10 mL total). The reaction mixture was stirred for 24 h, after which time the solvent was removed in vacuo to give a brown powder (70% yield). Both recrystallization over days at −30 °C from saturated hexanes, and slow evaporation of hexanes yielded thin red needles. The product sublimed between 100 and 120 °C at 5 mTorr and melted without decomposition between 161 and 165 °C. ^{1}H NMR: (C_6D_6) 8.1, 13.8, 21 (v broad) ppm; (d_8-toluene, 298 K) 8.1, 13.8, 21 (v broad) ppm; (d_8-toluene, 233 K) 4.9, 11.4, 12.9, 19 (v. broad) ppm. Vis: λ_{max} 481 nm. Anal. Found (calcd): C, 56.16 (56.60); H, 11.34 (11.02).

Reactions with H$_2$(g). Approximately 10 mg of each complex was dissolved in approximately 1 mL of C_6D_6 (with the exception of [{Mn(μ-$CH_2SiMe_3)_2$}$_\infty$], which was suspended in approximately 1 mL of d_8-toluene). The resulting solution (or suspension) was placed in a thick-walled NMR tube with a J. Young Teflon valve and was freeze−pump−thawed (×3). The NMR tube was then placed under an atmosphere of hydrogen gas, cooled to −95 °C using a liquid nitrogen/acetone bath, sealed at this low temperature, and warmed to room temperature to provide approximately 1.7 atm of hydrogen gas. Reactions were then observed by ^{1}H NMR spectroscopy as a function of time and temperature. Upon reaction completion, gases were removed by exposing to dynamic argon and solutions were decanted. Shiny metallic mirrors on the walls of the NMR tubes were sonicated into around 2 mL of toluene (rarely, the mirrors were physically scratched into suspension). The resulting silver-black powder was then washed twice with 5 mL of toluene and once with 5 mL of hexanes, dried in vacuo, and examined by PXRD.

Reactions with Diethylzinc. These reactions were conducted in a manner analogous to those with H_2, with the following modifications: approximately 10−15 mg of each manganese complex was used, and rather than addition of H_2, 1−3 equiv of neat diethylzinc was added to the solution (or suspension) in the NMR tube within the glovebox, and the Teflon valve was immediately closed to ensure that volatile reaction byproducts did not escape. The resulting silver mirrors were sonicated to yield silver-black powders (in most cases pyrophoric) which were examined by PXRD as well as XPS in some cases.

■ ASSOCIATED CONTENT

Supporting Information

The Supporting Information is available free of charge on the ACS Publications website at DOI: 10.1021/acs.organomet.5b00907.

Crystallographic details, X-ray structures of **5** (crystallized from toluene), **8**, and [{Mn(CH_2SiMe_3)(μ-

DOI: 10.1021/acs.organomet.5b00907
Organometallics 2016, 35, 168−180

$CH_2SiMe_3)(PEt_3)\}_2]$, UV/visible spectra, SQUID data and fits, Evans magnetic measurement data, ^1H NMR spectra of pure products and reactions with H_2 and $ZnEt_2$, and PXRD and XPS data (PDF)
Crystallographic data (CIF)

AUTHOR INFORMATION

Corresponding Author

*D.J.H.E.: tel, 905-525-9140; fax, 905-522-5209; e-mail, emslied@mcmaster.ca.

Notes

The authors declare no competing financial interest.

ACKNOWLEDGMENTS

D.J.H.E. thanks Intel Corporation for funding through Semiconductor Research Corporation (SRC). We are grateful to Paul Dube and Dr. Yurij Mozharivskyj for assistance with SQUID operation and analysis, Dr. Hilary Jenkins, Dr. Jim Britten, and Victoria Jarvis for assistance with single-crystal and powder X-ray diffraction, Megan Fair for running combustion elemental analysis, Allen Pauric for assistance in determining T_1 relaxation times and attempting DOSY NMR spectroscopy, and Dr. Rana Sodhi (Surface Interface Ontario) for running XPS on selected samples.

REFERENCES

(1) (a) Smith, D. L. *Thin Film Deposition: Principles and Practice*; McGraw-Hill: New York, 1995. (b) *Modern Electroplating*, 5th ed.; Schlesinger, M., Ed.; Wiley: Hoboken, NJ, 2014.

(2) (a) So long as the amount of precursor and coreactant delivered to the surface is sufficient to ensure complete reaction and maximum surface coverage, the film thickness will depend only on the number of precursor/purge/coreactant/purge cycles, even within high aspect ratio features. This is termed self-limiting growth, and if self-limiting growth cannot be achieved, the deposition method is pulsed CVD, rather than ALD. (b) For the remainder of this paper, ALD will refer exclusively to thermal ALD.

(3) (a) Ritala, M.; Niinistö, J. Atomic Layer Deposition. In *Chemical Vapour Deposition: Precursors, Processes and Applications*; Jones, A. C., Hitchman, M. L., Eds.; Royal Society of Chemistry: London, 2009; Chapter 4, pp 158−271. (b) Kääriäinen, T.; Cameron, D.; Kääriäinen, M.-L.; Sherman, A. *Atomic Layer Deposition: Principles, Characteristics and Nanotechnology Applications*; Scrivener Publishing: Salem, MA, 2013. (c) *Atomic Layer Deposition for Semiconductors*; Hwang, C. S., Ed.; Springer: New York, 2014. (d) *Atomic Layer Deposition of Nanostructured Materials*; Pinna, N., Knez, M., Eds.; Wiley-VCH: Weinheim, Germany, 2012. (e) Johnson, R. W.; Hultqvist, A.; Bent, S. F. *Mater. Today* **2014**, *17*, 236−246.

(4) (a) Knisley, T. J.; Kalutarage, L. C.; Winter, C. H. *Coord. Chem. Rev.* **2013**, *257*, 3222−3231. (b) Emslie, D. J. H.; Chadha, P.; Price, J. S. *Coord. Chem. Rev.* **2013**, *257*, 3282−3296.

(5) (a) Klaus, J. W.; Ferro, S. J.; George, S. M. *Thin Solid Films* **2000**, *360*, 145−153. (b) Grubbs, R. K.; Steinmetz, N. J.; George, S. M. *J. Vac. Sci. Technol., B: Microelectron. Process. Phenom.* **2004**, *22*, 1811−1821.

(6) (a) Kim, S.-H.; Hwang, E.-S.; Kim, B.-M.; Lee, J.-W.; Sun, H.-J.; Hong, T. E.; Kim, J.-K.; Sohn, H.; Kim, J.; Yoon, T.-S. *Electrochem. Solid-State Lett.* **2005**, *8*, C155−C159. (b) Kim, S.-H.; Kwak, N.; Kim, J.; Sohn, H. *J. Electrochem. Soc.* **2006**, *153*, G887−G893.

(7) Yang, M.; Chung, A.; Yoon, A.; Fang, H.; Zhang, A.; Knepfler, C.; Jackson, R.; Byun, J. S.; Mak, A.; Eizenberg, M.; Xi, M.; Kori, M.; Sinha, A. K. In *Conference Proceedings ULSI, XVII*; Materials Research Society: Conshohocken, PA, 2002; p 655.

(8) *CRC Handbook of Chemistry and Physics*, 92nd ed.; Haynes, W. M., Ed.; CRC Press: Boca Raton, FL, 2011−2012; pp 5−80 and 85−89.

(9) Thompson, D.; Anthis, J. W. Precursors and methods for the atomic layer deposition of manganese. WO2012125439A2, 2012.

(10) Kalutarage, L. C.; Martin, P. D.; Heeg, M. J.; Winter, C. H. *J. Am. Chem. Soc.* **2013**, *135*, 12588−12591.

(11) Kalutarage, L. C.; Clendenning, S. B.; Winter, C. H. *ECS Trans.* **2014**, *64*, 147−157.

(12) Klesko, J. P.; Thrush, C. M.; Winter, C. H. *Chem. Mater.* **2015**, *27*, 4918−4921.

(13) (a) Vidjayacoumar, B.; Emslie, D. J. H.; Clendenning, S. B.; Blackwell, J. M.; Britten, J. F.; Rheingold, A. *Chem. Mater.* **2010**, *22*, 4844−4853. (b) Vidjayacoumar, B.; Ramalingam, V.; Emslie, D. J. H.; Blackwell, J.; Clendenning, S. *ECS Trans.* **2013**, *50*, 53−66.

(14) (a) Lim, B. S.; Rahtu, A.; Gordon, R. G. *Nat. Mater.* **2003**, *2*, 749−754. (b) Lim, B. S.; Rahtu, A.; Park, J.-S.; Gordon, R. G. *Inorg. Chem.* **2003**, *42*, 7951−7958.

(15) Igumenov, I. K.; Semyannikov, P. P.; Trubin, S. V.; Morozova, N. B.; Gelfond, N. V.; Mischenko, A. V.; Norman, J. A. *Surf. Coat. Technol.* **2007**, *201*, 9003−9008.

(16) Dussarrat, C.; Gatineau, J. *Proc. Electrochem. Soc.* **2005**, *2005-05*, 354−359.

(17) Utriainen, M.; Kroger-Laukkanen, M.; Johansson, L. S.; Niinisto, L. *Appl. Surf. Sci.* **2000**, *157*, 151−158.

(18) (a) Senkevich, J. J.; Tang, F.; Rogers, D.; Drotar, J. T.; Jezewski, C.; Lanford, W. A.; Wang, G.; Lu, T. *Chem. Vap. Deposition* **2003**, *9*, 258−264. (b) Ten Eyck, G. A.; Pimanpang, S.; Bakhru, H.; Lu, T.-M.; Wang, G.-C. *Chem. Vap. Deposition* **2006**, *12*, 290−294.

(19) (a) Martensson, P.; Carlsson, J. O. *Chem. Vap. Deposition* **1997**, *3*, 45−50. (b) Martensson, P.; Carlsson, J.-O. *J. Electrochem. Soc.* **1998**, *145*, 2926−2931. (c) Li, Z.; Rahtu, A.; Gordon, R. G. *J. Electrochem. Soc.* **2006**, *153*, C787−C794. (d) Li, Z.; Barry, S. T.; Gordon, R. G. *Inorg. Chem.* **2005**, *44*, 1728−1735.

(20) Lee, B. H.; Hwang, J. K.; Nam, J. W.; Lee, S. U.; Kim, J. T.; Koo, S.-M.; Baunemann, A.; Fischer, R. A.; Sung, M. M. *Angew. Chem., Int. Ed.* **2009**, *48*, 4536−4539.

(21) Hierso, J.-C.; Feurer, R.; Kalck, P. *Chem. Mater.* **2000**, *12*, 390−399.

(22) (a) Aaltonen, T.; Ritala, M.; Sajavaara, T.; Keinonen, J.; Leskelae, M. *Chem. Mater.* **2003**, *15*, 1924−1928. (b) Aaltonen, T.; Ritala, M.; Tung, Y.-L.; Chi, Y.; Arstila, K.; Meinander, K.; Leskelae, M. *J. Mater. Res.* **2004**, *19*, 3353−3358.

(23) Alkyl complexes of more electropositive metals are typically more reactive towards σ-bond metathesis reactions: Waterman, R. *Organometallics* **2013**, *32*, 7249−7263.

(24) (a) Koike, J.; Wada, M. *Appl. Phys. Lett.* **2005**, *87*, 041911. (b) Usui, T.; Nasu, H.; Takahashi, S.; Shimizu, N.; Nishikawa, T.; Yoshimaru, M.; Shibata, H.; Wada, M.; Koike, J. *IEEE Trans. Electron Devices* **2006**, *53*, 2492−2499. (c) Haneda, M.; Iijima, J.; Koike, J. *Appl. Phys. Lett.* **2007**, *90*, 252107. (d) Au, Y.; Lin, Y.; Kim, H.; Beh, E.; Liu, Y.; Gordon, R. G. *J. Electrochem. Soc.* **2010**, *157*, D341−D345. (e) Lozano, J. G.; Lozano-Perez, S.; Bogan, J.; Wang, Y. C.; Brennan, B.; Nellist, P. D.; Hughes, G. *Appl. Phys. Lett.* **2011**, *98*, 123112.

(25) Hartwig, J. *Organotransition Metal Chemistry: From Bonding to Catalysis*; University Science Books: Sausalito, CA, 2010.

(26) (a) Ozin, G. A.; McCaffrey, J. G. *J. Am. Chem. Soc.* **1984**, *106*, 807−809. (b) Wang, X.; Andrews, L. *J. Phys. Chem. A* **2003**, *107*, 4081−4091.

(27) Clauss, K.; Beermann, C. *Angew. Chem.* **1959**, *71*, 627.

(28) (a) Andersen, R. A.; Carmona-Guzman, E.; Mertis, K.; Sigurdson, E.; Wilkinson, G. *J. Organomet. Chem.* **1975**, *99*, C19−C20. (b) Andersen, R. A.; Carmona-Guzman, E.; Gibson, J. F.; Wilkinson, G. *J. Chem. Soc., Dalton Trans.* **1976**, 2204−2211.

(29) Bochmann, M.; Wilkinson, G.; Young, G. B. *J. Chem. Soc., Dalton Trans.* **1980**, 1879−1887.

(30) Personal communication (ref 6) within ref 28b.

(31) Campora, J.; Palma, P.; Perez, C. M.; Rodriguez-Delgado, A.; Alvarez, E.; Gutierrez-Puebla, E. *Organometallics* **2010**, *29*, 2960−2970.

(32) Manzer, L. E.; Guggenberger, L. J. *J. Organomet. Chem.* **1977**, *139*, C34−C38.

DOI: 10.1021/acs.organomet.5b00907
Organometallics 2016, 35, 168−180

(33) Andersen, R. A.; Berg, D. J.; Fernholt, L.; Faegri, K., Jr.; Green, J. C.; Haaland, A.; Lappert, M. F.; Leung, W. P.; Rypdal, K. *Acta Chem. Scand.* **1988**, *42a*, 554−562.
(34) Buttrus, N. H.; Eaborn, C.; Hitchcock, P. B.; Smith, J. D.; Sullivan, A. C. *J. Chem. Soc., Chem. Commun.* **1985**, 1380−1381.
(35) Al-Juaid, S. S.; Eaborn, C.; El-Hamruni, S. M.; Hitchcock, P. B.; Smith, J. D.; Sozerli Can, S. E. *J. Organomet. Chem.* **2002**, *649*, 121−127.
(36) (a) Davies, J. I.; Howard, C. G.; Skapski, A. C.; Wilkinson, G. *J. Chem. Soc., Chem. Commun.* **1982**, 1077−1078. (b) Howard, C. G.; Girolami, G. S.; Wilkinson, G.; Thornton-Pett, M.; Hursthouse, M. B. *J. Chem. Soc., Dalton Trans.* **1983**, 2631−2637.
(37) Howard, C. G.; Wilkinson, G.; Thornton-Pett, M.; Hursthouse, M. B. *J. Chem. Soc., Dalton Trans.* **1983**, 2025−2030.
(38) (a) Girolami, G. S.; Wilkinson, G.; Galas, A. M. R.; Thornton-Pett, M.; Hursthouse, M. B. *J. Chem. Soc., Dalton Trans.* **1985**, 1339−1348. (b) Hitchcock, P. B.; Lappert, M. F.; Leung, W. P.; Buttrus, N. H. *J. Organomet. Chem.* **1990**, *394*, 57−67.
(39) Alberola, A.; Blair, V. L.; Carrella, L. M.; Clegg, W.; Kennedy, A. R.; Klett, J.; Mulvey, R. E.; Newton, S.; Rentschler, E.; Russo, L. *Organometallics* **2009**, *28*, 2112−2118.
(40) Riollet, V.; Coperet, C.; Basset, J.-M.; Rousset, L.; Bouchu, D.; Grosvalet, L.; Perrin, M. *Angew. Chem., Int. Ed.* **2002**, *41*, 3025−3027.
(41) Bart, S. C.; Hawrelak, E. J.; Schmisseur, A. K.; Lobkovsky, E.; Chirik, P. J. *Organometallics* **2004**, *23*, 237−246.
(42) Crewdson, P.; Gambarotta, S.; Yap, G. P. A.; Thompson, L. K. *Inorg. Chem.* **2003**, *42*, 8579−8584.
(43) Blair, V. L.; Clegg, W.; Conway, B.; Hevia, E.; Kennedy, A.; Klett, J.; Mulvey, R. E.; Russo, L. *Chem. - Eur. J.* **2008**, *14*, 65−72.
(44) Kennedy, A. R.; Klett, J.; Mulvey, R. E.; Robertson, S. D. *Eur. J. Inorg. Chem.* **2011**, *2011*, 4675−4679.
(45) Girolami, G. S.; Howard, C. G.; Wilkinson, G.; Dawes, H. M.; Thornton-Pett, M.; Motevalli, M.; Hursthouse, M. B. *J. Chem. Soc., Dalton Trans.* **1985**, 921−929.
(46) Complex **1** has previously been characterized crystallographically.[28b,39]
(47) Andersen, R. A.; Haaland, A.; Rypdal, K.; Volden, H. V. *J. Chem. Soc., Chem. Commun.* **1985**, 1807−1808.
(48) Meier, R. M.; Hanusa, T. P. In *Structural Organomanganese Chemistry*; Wiley: Chichester, U.K., 2011; pp 43−169.
(49) *CRC Handbook of Chemistry and Physics*, 95th ed.; Haynes, W. M., Ed.; CRC Press: Boca Raton, FL, 2014−2015; Section 9: Molecular Structure and Spectroscopy-Atomic Radii of the Elements.
(50) (a) Oberteuffer, J. A.; Ibers, J. A. *Acta Crystallogr., Sect. B: Struct. Crystallogr. Cryst. Chem.* **1970**, *26*, 1499−1504. (b) Preston, G. D. *Philos. Mag.* **1928**, *5*, 1207−1225. (c) Haglund, J.; Fernandez Guillermet, F.; Grimvall, G.; Korling, M. *Phys. Rev. B: Condens. Matter Mater. Phys.* **1993**, *48*, 11685−11691.
(51) Dunitz, J. D. *Perspectives in Structural Chemistry*; Wiley: New York, 1968; Vol. *II*.
(52) Hilderbrandt, R. L.; Wieser, J. D.; Montgomery, L. K. *J. Am. Chem. Soc.* **1973**, *95*, 8598.
(53) Dumke, A. C.; Pape, T.; Kösters, J.; Feldmann, K.-O.; Schulte to Brinke, C.; Hahn, F. E. *Organometallics* **2013**, *32*, 289−299.
(54) Attempts to determine whether the dimeric structure of complex **4** (Figure 3) remained intact in solution or dissociated into monometallic species using DOSY NMR failed due to very short T_1 relaxation times (the average for the three signals in complex **4** is 0.282 ms at 0.03 g/mL).
(55) Xu, Z.; Thompson, L. K.; Waldmann, O. *MAGMUN4.1*.
(56) (a) Evans, D. F. *J. Chem. Soc.* **1959**, 2003−2005. (b) Schubert, E. M. *J. Chem. Educ.* **1992**, *69*, 62.
(57) For **5**, 4 equiv of $SiMe_4$ was observed after the intermediate (**3**) had reacted with excess H_2 at 120 °C for 12 h.
(58) Complex **5** slowly decomposed to **3** at 120 °C in solution. However, this decomposition proceeded much more slowly than the reaction to form **3** in the presence of H_2.
(59) NMR signals for free dmpm were shifted by 0.05−0.1 ppm (^{1}H NMR) and 1−3 ppm (^{31}P NMR) relative to a reference sample.
(60) A small amount of an unidentified phosphorus-containing product was observed in the reaction of **3** with $ZnEt_2$ at 60 °C. This product was not observed in the reaction of **5** with $ZnEt_2$, most likely due to milder reaction conditions.
(61) Nakagawa, Y.; Hori, T. *Trans. Jpn. Inst. Met.* **1972**, *13*, 167−170.
(62) (a) Zhu, Z.; Wright, R. J.; Olmstead, M. M.; Rivard, E.; Brynda, M.; Power, P. P. *Angew. Chem., Int. Ed.* **2006**, *45*, 5807−5810. (b) Zhu, Z.; Brynda, M.; Wright, R. J.; Fischer, R. C.; Merrill, W. A.; Rivard, E.; Wolf, R.; Fettinger, J. C.; Olmstead, M. M.; Power, P. P. *J. Am. Chem. Soc.* **2007**, *129*, 10847−10857.
(63) Zhu, Z.; Fettinger, J. C.; Olmstead, M. M.; Power, P. P. *Organometallics* **2009**, *28*, 2091−2095.
(64) Greene, T. M.; Andrews, L.; Downs, A. J. *J. Am. Chem. Soc.* **1995**, *117*, 8180−8187.
(65) Flory, M. A.; Apponi, A. J.; Zack, L. N.; Ziurys, L. M. *J. Am. Chem. Soc.* **2010**, *132*, 17186−17192.
(66) ZnH_2 is reported to decompose to Zn and H_2 at 90 °C: Ashby, E. C.; Watkins, J. J. *Inorg. Synth.* **1977**, *17*, 6−9.
(67) Chadha, P.; Emslie, D. J. H.; Jenkins, H. A. *Organometallics* **2014**, *33*, 1467−1474.
(68) Burger, B. J.; Bercaw, J. E. Vacuum Line Techniques for Handling Air-Sensitive Organometallic Compounds. In *Experimental Organometallic Chemistry-A Practicum in Synthesis and Characterization*; American Chemical Society: Washington, DC, 1987; Vol. *357*, pp 79−98.
(69) Andersen, R. A.; Wilkinson, G. *Inorg. Synth.* **1979**, *19*, 262−265.
(70) Fulmer, G. R.; Miller, A. J. M.; Sherden, N. H.; Gottlieb, H. E.; Nudelman, A.; Stoltz, B. M.; Bercaw, J. E.; Goldberg, K. I. *Organometallics* **2010**, *29*, 2176−2179.
(71) Sheldrick, G. M. *Acta Crystallogr., Sect. A: Found. Crystallogr.* **2008**, *64*, 112−122.

DOI: 10.1021/acs.organomet.5b00907
Organometallics 2016, 35, 168−180